Journal of Marine Systems 109-110 (2013) S26–S44

Contents lists available at ScienceDirect

Journal of Marine Systems

journal homepage: www.elsevier.com/locate/jmarsys

Internal tide interactions in the Bay of Biscay: Observations and modelling

A. Pichon [a,*], Y. Morel [b,1], R. Baraille [b,1], L.S. Quaresma [c]

[a] Service Hydrographique et Océanographique de la Marine, Centre Militaire d'Océanographie, 13 rue le Chatellier, BP 30316, 29603 Brest Cedex, France
[b] Service Hydrographique et Océanographique de la Marine, Centre Militaire d'Océanographie, 14 avenue Edouard Belin, 31000 Toulouse, France
[c] Instituto Hidrográfico, Divisão de Oceanografia, Rua das Trinas, n. 49 1249-093 Lisboa, Portugal

ARTICLE INFO

Article history:
Received 2 September 2010
Received in revised form 6 June 2011
Accepted 1 July 2011
Available online 12 July 2011

Keywords:
Bay of Biscay
Internal tides
Internal solitary waves
HYCOM model

ABSTRACT

The paper addresses three-dimensional dynamics and interactions between internal waves in the Bay of Biscay, observed during an oceanographic survey conducted in summer 2006. These interactions are modelled and compared with observations. The effect of the internal tide (IT) beam structure in the deep ocean, on the interfacial IT along the seasonal thermocline, is analysed.

To determine the regions of strong three-dimensional interactions and explain the observed IT structures, numerical simulations are used. Model results and observations show evidence of IT following analytical ray paths, but also interactions between beams. IT currents higher than 0.20 $m.s^{-1}$, are measured at 3000 m near the bottom of the French continental slope, and are clearly modelled. In addition, in the mid-bay of Biscay, both the model and the data highlight a strong internal tidal current from 0 to a depth of 1500 m, generated by three-dimensional interactions.

Large interfacial ITs, associated with short wavelengths, are shown to be generated by deep ocean ITs when the latter reach the surface and impinge on the seasonal thermocline. It is indeed demonstrated that:

- In the model and in the observations, interfacial ITs are intensified where the beam of the deep ocean IT reaches the seasonal thermocline.
- The vertical variations of currents, measured in the surface layers, are related to short wavelengths observed in the seasonal thermocline, and also to the velocity modelled along the beam of the deep ocean IT.
- These short wavelengths are generated in the middle of the Bay of Biscay where the deep IT impinges on the seasonal thermocline.

Drifting thermistor chains were launched to follow the evolution of the seasonal thermocline. Along their trajectories, internal tide events occur at locations where the modelled surface tidal current has maximum values, and during spring baroclinic tides. The model clearly reproduces these events, but with a delay of one or two days compared to the observations. This delay is most likely due to a mixed layer too deep in the model.

1. Introduction

In the Bay of Biscay, there exist different areas of internal tide (IT) generation and the central Bay is a region where ITs are amplified because of their non-linear interactions (Azevedo et al., 2006; New and Pingree, 1990, 1992; Pichon and Correard, 2006). In this region, ITs were mainly described using two dimensional vertical plane configurations. Different models reproduced beams of energy in the deep ocean (Baines, 1982; Gerkema, 2001; New, 1988), and propagation of internal tides in the seasonal thermocline (Gerkema, 1996; Mazé, 1987; Pichon and Mazé, 1990; Pingree and Mardell, 1985). Observations showed the particular vertical distribution of the ITs in the deep ocean (Lam et al., 2004; Gerkema et al., 2004; Pingree and New, 1989, 1991; Jezequel et al. 2002) as well as interactions between the deep ocean IT and the seasonal IT in the central Bay (New and Pingree, 1990, 1992). However, the particular topography of the Bay generates many interactions, which produce a complex three-dimensional distribution of the internal tides. The main generation areas are located along the French and Spanish shelf breaks. In the northern Bay, the tide is subject to the effect of the English Channel, with an amplification of the tidal current on the northern French continental shelf. Steep

* Corresponding author. Tel.: +33 2 98 22 15 68.
E-mail addresses: pichon@shom.fr (A. Pichon), morel@shom.fr (Y. Morel), baraille@shom.fr (R. Baraille), quaresma@gmail.com (L.S. Quaresma).
[1] Tel.: +33 5 61 33 29 32.

0924-7963/$ – see front matter © 2011 Elsevier B.V. All rights reserved.
doi:10.1016/j.jmarsys.2011.07.003

topography and local canyons increase the barotropic vertical velocity at the origin of the internal tide forcing. High internal tides were modelled and observed at the top of the continental slope, from 47°N to 49°N (Pingree et al., 1986; Pingree and Mardell, 1985; Serpette and Mazé, 1989). More recently, another generation region was observed in the southern Bay of Biscay near Cape Ortegal. Maximum values of the IT barotropic forcing term were found at the Spanish shelf break between 8°W and 9°W and by 44.2°N (Azevedo et al., 2006; Pichon and Correard, 2006). Some observations of internal solitary waves (ISWs), during summer in the central Bay region were attributed to this latter generation area (Da silva et al., 2007; New and DaSilva, 2002). The relationship between the ISW packets in the central Bay and generation spots over the Spanish slope, was checked by plotting the ITs' energy ray paths. The ISWs generation is due to an increase of the interfacial internal tide in the region where the deep ocean internal tides emerge at the surface. Interactions between the deep ocean ITs and the internal tide at the base of a mixed layer are produced by resonance between the frequency σ, of the deep ocean ITs, and the frequency σ_0 of the wave propagating at the interface, i.e. the thermocline (Thorpe, 1998). When resonance is reached, non-linear effects increase at the thermocline, where the deep ocean linear wave is reflected by higher stratification. Non-linear interactions were also studied with different stratifications of the Bay of Biscay by Gerkema (2001). He found that, even in the linear case, the amplitude of the interfacial wave is increased for typical values of stratification in the deep ocean and in the seasonal thermocline (especially in summer). When non-linear terms are introduced, solitary waves are then generated by two processes: first, the scattering of the deep ocean beam when it is reflected at the thermocline, and second, the disintegration of the interfacial wave in "solitons", when non-linear effects are sufficiently strong. The ISWs, therefore, are generally expected and observed where strong ITs impinge on the seasonal thermocline.

Following Xing and Davies (1996, 1998) and Holloway (2001), the aim of the present study is to achieve three-dimensional modelling, compared with observations, to determine the location and mechanisms of IT amplification. To investigate three-dimensional interactions between different beams, the numerical model is based on the HYCOM (Bleck, 2002) adapted to the tidal processes (Morel et al., 2008; Pichon and Correard, 2006). The results are then confirmed by new observations, collected in two different areas of the central Bay of Biscay, and at the base of the continental slope. Moreover, IT propagation in the thermocline during the summer months is demonstrated, and correlated to the modelled surface velocity.

This paper is set out as follows. In Section 2, in situ data as well as the model configurations are presented. In Section 3, model results are detailed and compared with the ADCP and CTD observations. First, the spatial distribution of the internal tide forcing term is presented in Section 3.1, to show the influence of the Bay of Biscay topography on IT generation. In Section 3.2, two schematic simulations provide information on the interactions between waves by the transient state analysis (for the baroclinic modes) compared with steady IT spatial distribution. On the basis of the IT forcing term, three sections are chosen to explain the three-dimensional interactions between waves in the vertical plane (Section 3.3). Model results are validated in Section 3.4 at three particular locations, where the measurements show IT interactions. In Section 3.5 the outcrop of the IT beam energy is demonstrated in the observations and model results. The interactions of the deep ocean beams with the thermocline are described in Section 3.6, and comparisons with observations are made in Section 3.7. Finally, in Section 3.8, the effect of summer stratification on the internal tide evolution is addressed, using realistic model results. In Section 3.9, some perspectives are proposed in order to improve the internal tide modelling.

2. Material and method

2.1. Data

In July 2006, a SHOM (French Hydrographic and Oceanographic Service) experiment was conducted to study the regions where three-dimensional interactions produce an amplification of ITs. Data was collected in an area (Fig. 1) where the internal tide energy displayed a maximum value in the Bay of Biscay. Different measurements were also taken to describe both the spatial and temporal evolutions of the mixed layer thickness evolution under the action of ITs.

Three fixed point observations, PF1 to PF3, were positioned based on previous model results (Pichon and Correard, 2006). The first location, PF1 (6.5°W, 47°N) was along a downward beam coming from the French shelf break, on the continental slope at 3000 m depth. The points PF2 (7.2°W, 45.97°N) and PF3 (6.86°W, 46.62°N) were respectively positioned along the second and first reflections of the beam crossing point PF1. At these three locations, vertical density and velocity profiles were collected for two tidal cycles around the spring barotropic tide, ST (PF1 at ST, PF2 three days after ST, PF3 one day after ST): repeated CTD/LADCP stations measured the amplitude of the ITs and their effect on horizontal circulation. To obtain a time resolution of nearly 1 h, only the first 2800 m depth from the sea surface were sampled.

To measure the ISWs in the thermocline and vertical variations of velocity, different sections were taken around the PR1 and PR2 regions where non-linear interactions are expected to be more intense (see Fig. 1). A CTD mounted in a SEASOAR ocean undulator (Allen et al., 2002) was towed behind the ship. To reach a high spatial resolution (~1 km), the vertical range of the SEASOAR undulations was reduced to the first 200 m. Data collected by vessel mounted acoustic Doppler current profilers (VMADCP) at 150 kHz and 38 kHz frequencies were available at different vertical resolutions. Bin sizes of 8 m (150 kHz) and 24 m (38 kHz) were used (http://www.rdinstruments.com/). Vertical velocity profiles were collected every 2 min along the tracks, with a ship speed of about eight knots. The horizontal resolution, therefore, was less than 1 km.

The variations of velocity produced in the horizontal plane by the IT inside the seasonal thermocline, as well as in the vertical plane by the solitary waves, were measured by the high horizontal and vertical

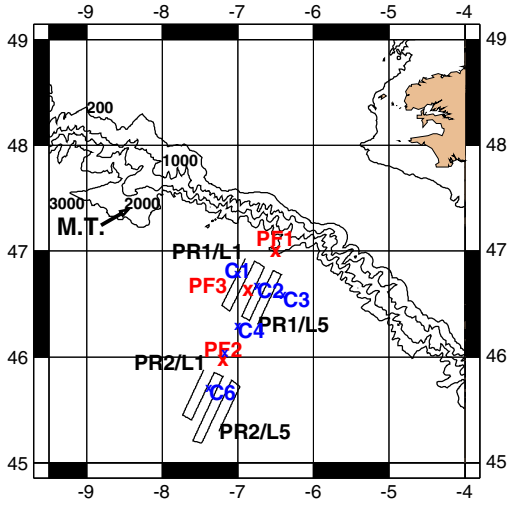

Fig. 1. Topography of the French continental slope and data collected in July 2006. M.T., Meriadzeck Terrace (bottom depth from 2000 m to 3000 m). PF1, PF2 and PF3 (red): CTD/LADCP stations on two tidal cycles. C1 to C6 (blue): initial position of the drifting thermistor chains. SEASOAR and VMADCP sections (L1 to L5) in the PR1 and PR2 regions (black).

resolutions of the first 300 m (150 kHz). The vertical range of the low frequency ADCP (1000 m), allowed a description of the velocity structure along the deep ocean beams.

Finally, drifting thermistor chains were launched in the same area (Fig. 1). With a vertical resolution of 10 m in the first 100 m, and a time range of 30 min, the temperature evolution was measured for three months from July to September 2006. The distribution of the mixed layer and the seasonal thermocline covered all the southern Bay of Biscay, below 47°N. Drifting buoys drogued at 15 m and 75 m were also launched at the same locations (C1 to C6) as the thermistor chains.

2.2. Model

The hybrid coordinate ocean model HYCOM (Bleck, 2002) is used with modifications to introduce the surface tide as forcing at the boundaries (Pichon and Correard, 2006). New numerical schemes are used in the barotropic equations, to improve the tide modelling in wet and dry regions close to the coast (Morel et al., 2008). The extension of the model covers the French area from 43°N to 51°N and from 15°W to the coast, at a resolution of 2 km. At the open boundaries and as initial conditions, the first main semi-diurnal components M2, S2, N2, K2 of the Toulouse Unstructured Grid Ocean model (T-UGOm or MOG2D, see Pairaud et al., 2008 and references therein) are introduced.

To analyse the density and velocity structure measured in July 2006 during the survey, two different configurations are developed.

In the first configuration, only the tidal processes are modelled. Isopycnal coordinates are used in an adiabatic mode, without diffusion of density, temperature and salinity. No surface atmospheric fluxes are introduced. Initial density is homogeneous in the horizontal plane. The initial condition of the velocity field is defined by the barotropic tide. The model starts on July 2, 2006. The baroclinic part of the tidal current is relaxed to zero at the open boundaries by using a sponge layer (see hereafter). A vertical stratification profile is defined using a time average of CTD stations collected in July during the experiment (Fig. 2). Thirty two isopycnal layers of different thickness are used. Fifteen layers represent the first 200 m, and sixteen layers of variable thickness (from 120 m to 200 m) define the stratification down to 3400 m. This configuration named hereafter the SCHEM–HYCOM model, is used with one (M2) or four tidal waves (M2, S2, N2, K2) applied at the open boundaries.

In the second configuration, hybrid coordinates are used. The ECMWF 0.5° resolution atmospheric fluxes are interpolated on the HYCOM grid, with a time resolution of 6 h over the year 2006. The K-profile parameterization (KPP) of Large et al. (1994) is used to represent the mixed layer evolution. Initial conditions of density are defined by the global ORCA-R025 configuration of the Mercator model including the sea surface evolution (Barnier et al., 2006) named hereafter 'MERCATOR'. The initial velocity field consists of two parts: the geostrophic current balanced with the MERCATOR density projected on the HYCOM grid, and the barotropic tidal current. The model starts on January 4, 2006. At the open boundaries, the barotropic mode is forced by the sum of the tidal flux, MERCATOR flux and rivers flux. The baroclinic variables are relaxed every seven days towards the MERCATOR fields. The baroclinic tidal current is therefore relaxed to zero at the open boundaries (since the MERCATOR model does not take into account tidal processes). The size of the sponge layer and the relaxation coefficient are chosen to damp both the baroclinic tidal waves (Pichon and Correard, 2006), and the meso-scale circulation modelled by HYCOM but not present in the MERCATOR fields.

The vertical grid uses isopycnal coordinates in the deep layers and a hybrid set of coordinates in the upper layers, adapted to the seasonal evolution of the mixed layer. Sixteen isopycnal layers are defined between 300 m and 3400 m. The density of each isopycnal layer is defined from a mean vertical density profile (an average in space and time over the year 2006 of the MERCATOR density field in the mid-bay of Biscay). On this profile, a "reference density" is chosen every 200 m. This choice limits the thickness of each layer (to approximately 200 m) which is important to accurately represent the ray paths of internal tide energy in the deep layers. Fifteen hybrid layers are used from the surface down to 300 m. The vertical grid is adapted to follow the seasonal variation of the mixed layer thickness (200 m in winter and 20 m or less in summer), while keeping the isopycnal coordinates inside the seasonal thermocline in summer (especially when gravity waves such as internal tides occur). The vertical resolution of the 'z' layers (mixed layer) and the reference density of the isopycnal layers (seasonal pycnocline) are controlled by two characteristic depths, which follow a monthly variation: the base of the mixed layer, MLD, and the base of the thermocline, THCD. The data points of MLD and THCD are bound by a threshold value of $3.10^{-3}\ s^{-1}$ on the monthly Brunt-Väisälä profile N(z), coming from the MERCATOR density averaged in space. In winter, MLD reaches 150 m and THCD, 250 m. The vertical resolution "dz" varies from 1 m to 5 m in summer, to 10 m in winter. This hybrid configuration is named hereafter the REAL–HYCOM model.

In both configurations, to compare the results with in situ observations, the model outputs are interpolated at the time and location of the different Seasoar/VMADCP sections, and along the trajectory of the drifting thermistors. Indeed, there is a Doppler effect on the observed IT wavelengths, since the phase celerity of the internal waves is of the same order of magnitude as the speed of the ship. Processing of the model outputs removes the bias related to the high temporal and spatial variability of the data field.

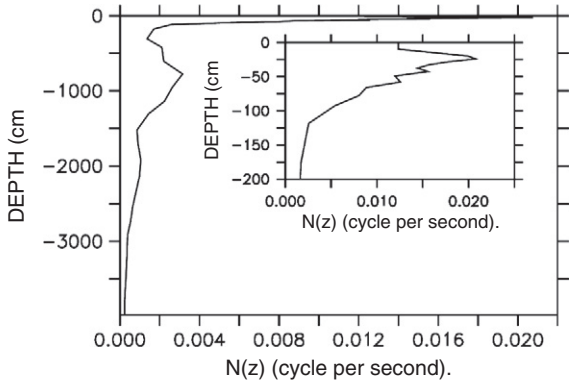

Fig. 2. Brunt-Väisälä frequency profile N(z), used in the SCHEM–HYCOM model, defined with an average of CTD data in July 2006. N (z) reaches 21 $10^{-3}\ s^{-1}$ in the seasonal pycnocline (24 m), 3.1 $10^{-3}\ s^{-1}$ in the permanent pycnocline (800 m) and $3.10^{-4}\ s^{-1}$ at 3400 m.

3. Results and discussion

The IT modelled by the SCHEM–HYCOM configuration under summer stratification, generates variations in the spatial distribution of the surface baroclinic velocity (Fig. 3). To analyse these variations, baroclinic wavelengths are calculated with the vertical Brunt-Väisälä profile used in the SCHEM–HYCOM model. The phase celerity of the mode 'n' is:

$$C_{\sigma,n} = \frac{C_n}{\sqrt{1-\left(\frac{f^2}{\sigma^2}\right)}} \quad (1)$$

where C_n is the eigenvalue of the vertical normal mode n, and $\lambda_{\sigma,n}$ is the corresponding wavelength. The characteristics of the main energetic modes are described in Table 1.

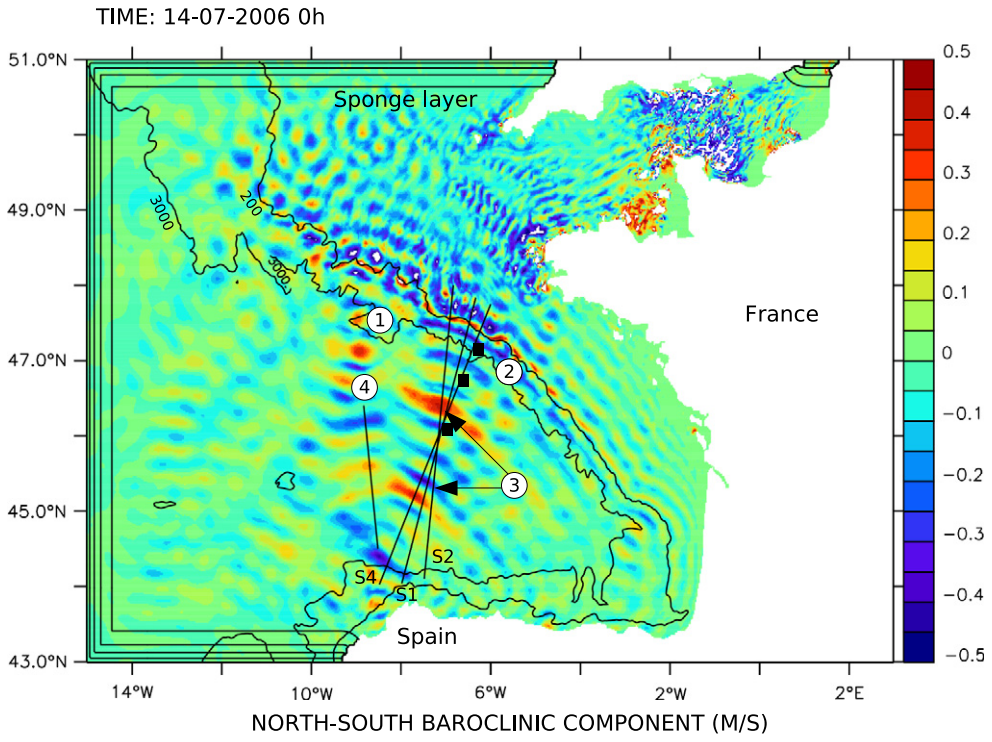

Fig. 3. North–south surface baroclinic velocity on July 14 2006 (SCHEM–HYCOM solution), in spring barotropic tide. The component varies from ±30 cm/s, mainly at the wavelength of the interfacial mode. 1: Meriadzeck Terrace. 2: French continental slope. 3: Regions in the central Bay of Biscay where ITs are expected to outcrop the surface. 4: SAR section with location of the ISWs packets, described in Da Silva et al. (2007). Black squares: position of the three fixed points. S1, S2, S4: vertical sections where the modelled solution is extracted. At the open boundaries, black lines are the damping coefficient values (from 0 to 5.10^{-5} s^{-1} every 10^{-5} s^{-1}) applied in the sponge layer.

In addition, an interfacial IT in the seasonal thermocline is defined by a two layer approximation of the vertical density profile in the surface layers (from 0 to 200 m, Fig. 2):

$$C_\sigma = \sqrt{\frac{g'.h_0 \cdot (H - h_0)}{H.\left[1 - {}^{f^2}/_{\sigma^2}\right]}} \quad (2)$$

where g′ is the reduced gravity, h_0 the mean depth of the thermocline, H, the bottom depth, f the inertial frequency (Pichon and Mazé, 1990). The variation of the interfacial IT phase celerity with topography is detailed in Table 2. This interfacial IT is introduced to interpret the action of the seasonal thermocline on the wavelength variations modelled over the continental shelf.

The wavelength of this interfacial IT varies from 20 km (H = 40 m) to 40 km (H = 150 m) and is slightly increased to reach 50 km when H = 4000 m (see Table 2, the different phase celerity and wavelengths). As described in Table 1, this interfacial IT corresponds to the mode 2 in the deep ocean.

Table 1
Phase celerity $C_{\sigma,n}$ for the three first normal modes (n = 1, 2, 3), over a flat abyssal plain (H = 4000 m). The vertical Brunt-Väisälä profile of the SCHEM–HYCOM model is used (Fig. 2). $\lambda_{\sigma,n}$, is the corresponding wavelength.

	Mode number		
	1	2	3
M2:C_σ ($m.s^{-1}$)	2.68	1.15	0.80
λ_{M2} (km)	119.90	51.46	35.82
M4:C_σ ($m.s^{-1}$)	1.87	0.80	0.56
λ_{M4} (km)	41.91	17.99	12.52

Over the continental shelf, the surface baroclinic velocity follows spatial variations at the wavelength of the interfacial mode, from 20 km to 40 km (see Table 2). Over the abyssal plain, strong currents of ±0.30 $m.s^{-1}$ are modelled. This variability mainly follows the interfacial wavelength of about 50 km (Table 2). The signature of the "deep ocean" baroclinic modes (λ_1 = 120 km, λ_2 = 52 km, see Table 1) is also observed in two regions of the central Bay where the surface velocity reaches maximum values (0.5 $m.s^{-1}$). These areas, spaced by 135 km, i.e. close to the wavelength of the first deep ocean mode (120 km), correspond to regions where deep ocean internal tides are expected to emerge at the sea surface. In the central Bay, the baroclinic surface velocity shows interactions between waves, with an increase in current along a main axis of propagation (lines S1 to S4 in Fig. 3), already described with in situ data and SAR images (New, 1988; New and Pingree, 1990, 1992; Pingree and New, 1995). The baroclinic surface velocity is also strong along the SAR section described in Da silva et al., 2007("SAR" section (4) in Fig. 3). On this section, by 46°N, internal waves coming from the Spanish slope interact with the waves coming from the Meriadzeck Terrace (area (1) in Fig. 3).

3.1. The internal tides forcing term

Three dimensional interactions between waves will be analysed, first by the IT spatial distribution at different level depths (Section 3.2) and then by the vertical internal tide structure in three vertical sections S1, S2, S4 (Section 3.3). S1, S2 and S4 are chosen on the basis of the IT forcing term amplitude over the French and Spanish shelf breaks (Fig. 4). Along these sections, waves generated over the Spanish slope and/or reflected by this continental slope are expected to have a different effect on the IT amplitude.

The main baroclinic tide generation regions are revealed by the spatial distribution of the forcing term F, function of the barotropic

Table 2
Phase celerity C_σ and wavelength λ_{Mi} of the interfacial mode inside the seasonal thermocline defined by a two-layer approximation of the density profile in the surface layers (from 0 to 200 m, Fig. 2).

H (m)	42.15	48.5	55.8	67.1	75.85	88.3	109.2	148.3	4000
h_0 (m)	27.50	29.4	32.6	34.6	36.7	38.50	39.5	40.9	40.9
g′ ($m.s^{-2}$)	$7.85.10^{-3}$	8.8610^{-3}	$1.02.10^{-2}$	$1.11.10^{-2}$	$1.18.10^{-2}$	$1.24.10^{-2}$	$1.27.10^{-2}$	$1.30.10^{-2}$	$1.30\cdot10^{-2}$
M2:C_σ ($m.s^{-1}$)	0.42	0.49	0.57	0.67	0.73	0.80	0.88	0.96	1.12
λ_{M2} (km)	18.95	22.16	25.75	29.87	32.74	35.88	39.17	43.01	50.28
M4:C_σ ($m.s^{-1}$)	0.3	0.34	0.40	0.46	0.51	0.56	0.61	0.67	0.79
λ_{M4} (km)	6.6	7.7	9.00	10.4	11.4	12.5	13.7	15.0	17.6

current, the topography and the stratification. Following Baines, 1982, this body force F, at the origin of the internal tide, can be expressed as:

$$F = -\frac{2\pi \cdot z \cdot N^2(z)}{\sigma \cdot H^2}\left[Q_x \cdot \frac{\partial H}{\partial x} + Q_y \cdot \frac{\partial H}{\partial y}\right] \quad (3)$$

The vertical z-axis is positive upward with the ocean free surface at $z = 0$. Q (Qx, Qy) is the barotropic flux vector, H the topography, N(z) the Brunt-Väisälä frequency and σ, the tidal frequency (Azevedo et al., 2006; Sherwin et al., 2002; Xing and Davies, 1998). With the M2 and S2 velocities of the HYCOM model used in a barotropic mode, and the Brunt-Väisälä frequency of the SCHEM–HYCOM model, the body force

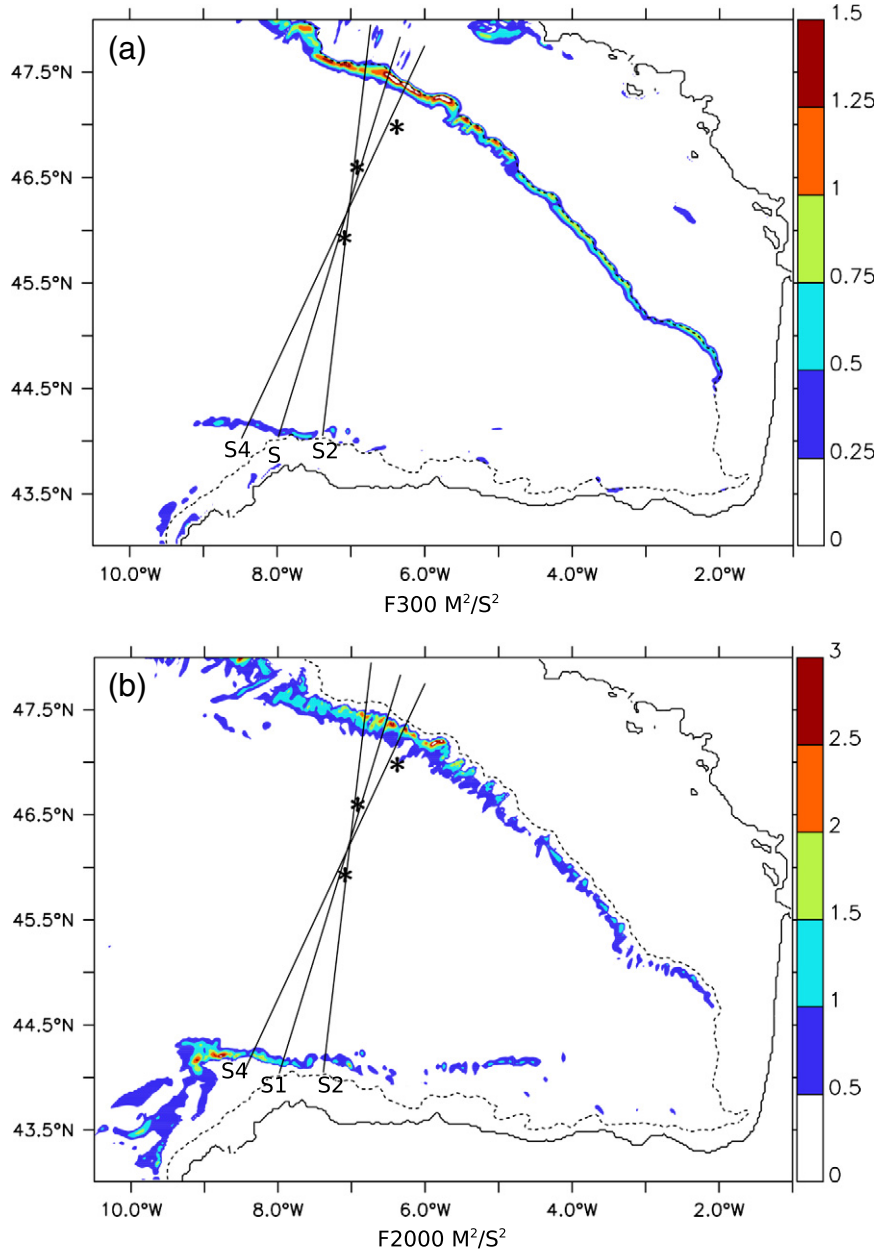

Fig. 4. Depth-integrated body force with the M2 and S2 waves. (a) vertical integration in the first three hundred metres (F300). (b) Vertical integration from 300 m to 2000 m (F2000). Near the French shelf break F300>1.25 $m^2.s^{-2}$ is three times higher than on the Spanish shelf break between S1 and S2 (F300 = 0.5 $m^2.s^{-2}$). F2000 (4b) is maximum (2.5 $m^2.s^{-2}$) by 9 W, along the isobath 1000 m. By 7.5 W and along S2, F2000 is lower than 0.5 $m^2.s^{-2}$. Stars in black: position of the three fixed points.

is integrated over the first 300 m (F300, Fig. 4a), and from 300 m to 2000 m (F2000, Fig. 4b). These two depth-integrated values distinguish the action of the seasonal pycnocline from the deep-persistent-stratification, on the internal tide generation.

Since "N" has no variation in the XY plane, the spatial distribution of F300 (Fig. 4a) is close to the spatial distribution of the barotropic forcing term (Pichon and Correard, 2006).

The internal tide forcing term near the French shelf break between 46.5°N and 48°N (F300>1.25 $m^2.s^{-2}$), is twice or three times larger than the one at the Spanish shelf break between S1 and S2 (F300 = 0.5 $m^2.s^{-2}$). The southern part of section S2 is at the edge of the latter area of generation, where the internal tide forcing is weak (Fig. 4b). The differences in the spatial distribution of F300 and F2000 along the Spanish continental slope (Fig. 4b), show the influence of deep layer stratification on the internal tide generation. Indeed, in Fig. 4b, close to the southern edge of section S4, F2000 reaches a maximum value of 2.5 $m^2.s^{-2}$ by 9°W, along the 1000 m isobath. This spatial distribution suggests that the permanent pycnocline has an influence on the generation of the internal tides propagating along the SAR section (Fig. 3) and, as a consequence, on the generation of ISW packets (Da silva et al., 2007). In Fig. 4b, between S1 and S2 by 8°W, F2000 is weak (it reaches a value close to 1.5 $m^2.s^{-2}$ as in Azevedo et al. (2006). In conclusion, the generation areas along the Spanish slope, will mainly affect the southern edge of the sections S1 and S4 and only weakly section S2.

3.2. Three-dimensional interactions on the horizontal plane

Three-dimensional interactions can locally increase internal tides in different regions of the Bay of Biscay. The analysis of the modelled transient state helps to define the areas of influence for waves coming from either the French or Spanish continental slopes. The generation of high internal tide amplitude in the central Bay, and the relative importance of these two systems of waves, are described by using model simulations forced by different topography. The SCHEM–HYCOM model, starting at rest for the baroclinic modes, is forced with a single tidal harmonic (M2), and a real (RT) or schematic topography (ST). The ST topography is built as follows: between 45°N and 48.5°N, the real French continental slope is modified. A "scheme-slope" with a uniform width corresponding to the mean width of the real French continental slope is introduced. The analytical topography from $H_{max}(x_{max}) = 4000$ m to $H_{min}(x_{min}) = 200$ m is expressed as:

$$H(x) = H_{max} - (H_{max} - H_{min}) * (\sin(u)/u)^2 \quad (4)$$
$$\text{with } u = (x - x_{min}) * \pi / (x_{max} - x_{min}).$$

Along this French uniform continental slope, internal tides are expected to be generated in phase during the transient state. Since the topography of the Spanish continental slope is not modified, the schematic topography configuration helps, by comparison with the RT simulation, to separate the origin of the different waves and the regions of influence of the two French and Spanish continental slopes. Moreover, the differences in the transient state of both the RT and ST cases provide information distinguishing the internal tides generated by the strength of the barotropic forcing term over the Spanish continental slope from the internal tides coming from the French shelf break and then reflected over the Spanish slope.

In both RT and ST configurations, the model starts with the same barotropic current. The spatial distribution of M2 internal tide amplitude and phase at 2500 m are then extracted from the SCHEM–HYCOM outputs after five and ten tidal periods (5 T, 10 T, Fig. 5a to h) during the transient state, and after thirty periods to reach a steady state (30 T, Fig. 5i to k). The patterns observed in Fig. 5 correspond to a horizontal cut through multiply reflected beams coming from either the French or the Spanish continental slopes (as discussed in more detail in Section 3.3).

After five tidal periods, the M2 internal tide amplitude is greater between 46°N and 48°N than in the southern or northern part of the Bay, whatever the topography (Fig. 5a and c). The distribution of the barotropic current in the Bay of Biscay, modified by the English channel (Pairaud et al., 2008; Pichon and Correard, 2006), is at the origin of the increasing barotropic forcing term (Fig. 4a, b) and consequently of the high internal tide amplitude between these two latitudes. In the RT case, two maxima of M2 IT amplitude (~60 m) are focussed by 7°W 47°N and by 6°W 46.8°N (Fig. 5a). On the contrary, in the ST case the spatial distribution of the M2 IT amplitude is uniform (Fig. 5c). In the RT case, positive interferences are observed over the plain by 7°W, 46°N just after 5 T (close to point PF2, the IT amplitude reaches 30 m, see Fig. 5a), and are increased after 10 T (in Fig. 5e the internal tide amplitude reaches 50 m). This interference produced by the difference in the orientation of the French continental slope, is not present in the ST case where all tidal waves coming from the French shelf break have the same propagation direction (Fig. 5c and g).

A distinction between ITs generated locally over the Spanish continental slope (named hereafter "Spanish" IT) and those generated over the French continental slope and then reflected over the Spanish continental slope (named hereafter "French" reflected IT) can be carried out with the M2 internal tidal amplitude distribution around 8.5°W, 44.5°N (RT case Fig. 5a, e, i, ST case Fig. 5c, g, k). After 5 T, at this point, the IT amplitude by 2500 m is quite the same order of magnitude in both RT (Fig. 5a) and ST (Fig. 5c) cases. During this transient state, the "French" IT incident has not yet propagated into the Spanish slope. Since the topography of the Spanish slope is similar in both cases, the effect of the local barotropic forcing term over the Spanish slope on the generation of an IT of an amplitude of nearly ~20 m to 30 m, by 8.5°W 44.5°N (Fig. 5a, c), is therefore confirmed. Now, after 10 T (Fig. 5e, g) and 30 T (steady state, Fig. 5i, k), the internal tide amplitude, by 8.5°W 44.5°N, is clearly different in the two RT and ST cases, with a maximum value of more than 80 m in the RT case after 30 T (Fig. 5i) and less than 60 m in the ST case (Fig. 5k). The increasing of the internal tide amplitude on the Spanish continental slope is therefore produced by the "French" internal tides reflected by the Spanish topography. This effect is reinforced by the geographic curve of the French continental slope: the "French" ITs generated between 46.5°N and 47.5°N are reflected on the Spanish slope in the RT case but not in the ST case.

The propagation direction of the different wave systems can be analysed with the spatial distribution of the M2 internal tide phase. The successive red–blue lines from Northeast to Southwest denote waves coming from the French shelf break. The successive red–blue lines from Southeast to Northwest, or from West to East, denote waves coming from the Spanish shelf break. After 5 T, the spatial distribution of the phase in the two cases clearly shows the Spanish wave coming from 8.5°W 44.5°N, which then propagates eastwards. The phase variation at the 8°W 44.5°N point (Fig. 5b and d), related to the amplitude of the wave (Fig. 5a, c), can identify the area of influence of the Spanish wave (see black/white dashed lines in Fig. 5a to h).

After 30 T (Fig. 5j, l) the phase distribution shows the action of the French waves reflected over the Spanish slope in the RT case but not in the ST case. In the real topography case (RT), the French incident waves coming along the (A) line direction are then reflected on the Spanish slope and a part of the energy is propagated along the (B) line (Fig. 5i, j). These reflections produce several maximum spots in the amplitudes along the SAR line (Fig. 3) where the waves coming from the Spanish slope interact with the waves coming from the Meriadzeck Terrace.

The distribution of the M2 internal tide amplitude, very different in the two topography cases, shows the action of the French slope orientation on the great internal tidal amplitude by 2500 m close to point PF2. This French slope configuration also amplifies the effect of the "French" IT reflected over the Spanish continental slope. These reflected waves increase the IT amplitude along the SAR line, and also

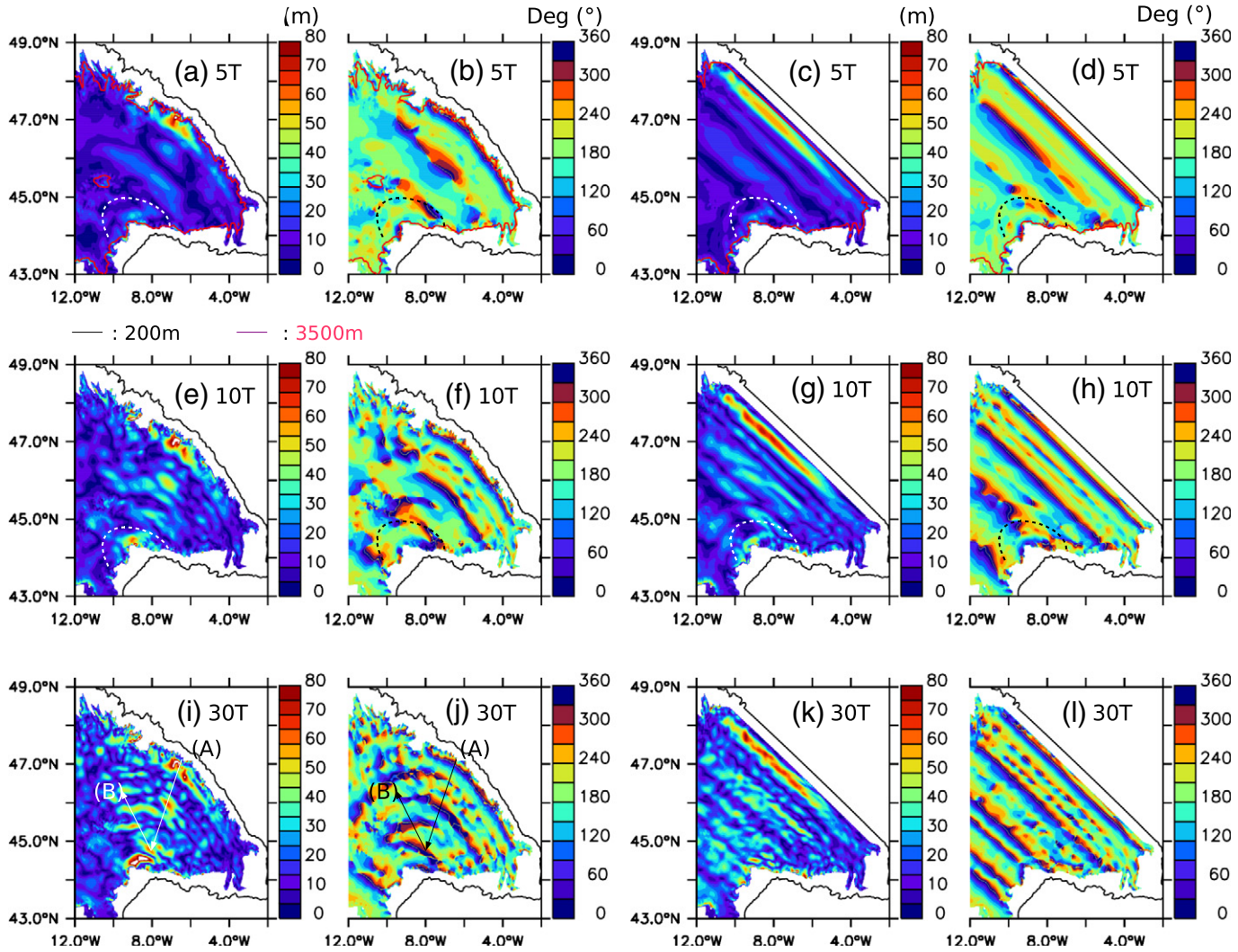

Fig. 5. M2 internal tide amplitude and phase at level depth 2500 m, extracted from SCHEM–HYCOM output: REAL–TOPOGRAPHY case RT (a, b, e, f, i, j), and SCHEM–TOPOGRAPHY case ST (c, d, g, h, k, l). Transient state is described with outputs after five (a, b, c, d) and ten M2 tidal periods (T) (e, f, g, h). Steady state is described with outputs after 30 T (i, j, k, l). Dashed lines (figures a to h): region of influence of internal tides generated over the Spanish slope. Lines A and B: main directions of propagation of the incident (A) and reflected (B) French IT.

near point PF2 (see the difference of IT amplitude by 7°W 46.0°N after 10 and 30 tidal periods Fig. 5e and i). The IT solution around point PF2 is therefore a combination of the effects of a direct propagation of waves from the French slopes and the reflections of these from the Spanish slopes.

3.3. Three-dimensional interactions on vertical sections

To interpret the model results and the observations, the distribution of the internal tide in the vertical plane is described along the three sections S1, S2 and S4. From the SCHEM–HYCOM model results, using the four semi-diurnal tidal waves, a Fourier analysis of each isopycnal level is performed over forty tidal periods of each harmonic. The vertical deviation of each isopycnal level referenced at its initial depth on July 2, 2006, gives the vertical amplitude of the internal tide at each frequency. As an example, the vertical amplitude of the M2 internal tide is plotted along the three vertical sections in Fig. 6 (S1), Fig. 7 (S2) and Fig. 8 (S4). The location of the three points PF1 to PF3 and the ray paths for the two-dimensional approximation are plotted in the figures. In this case, the slope "c" horizontal to the characteristic rays of the internal tide energy can be approximated by:

$$c(z) = \sqrt{\frac{\sigma_{M2}^2 - f^2}{N^2(z)}} \text{ from } z = 0 \text{ to } z = -H. \quad (5)$$

Indeed, the HYCOM uses primitive equations with a hydrostatic approximation which corresponds to $N^2 \gg \sigma^2_{M2}$. This approximation is justified at semi-diurnal frequencies (the relationship between the hydrostatic approximation and the ratio $\frac{N^2}{\sigma^2}$ is well described in Garrett and Gerkema, 2007). The beams trajectory is then defined by:

$$\sum_{1}^{n} c^{-1}(k).dh_k \quad (6)$$

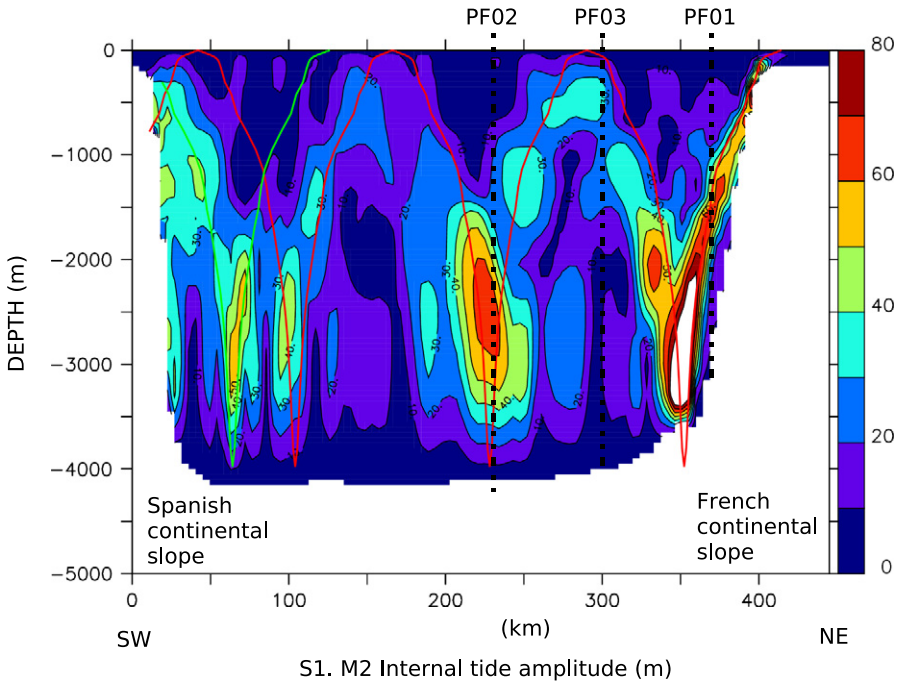

Fig. 6. Section S1. M2 internal tide amplitude (m) from the SCHEM–HYCOM model. In red, 2D analytical beam coming from the French shelf break (on the right). The first red beam crosses PF1 between 2000 m and 3000 m. At PF3 maximum IT occurs at 1000 m. In green, 2D analytical beam coming from the Spanish shelf break (on the left).

where c(k) is calculated by the Brunt-Väisälä frequency in the "n" layers of thickness dh_k. The comparison between the beam positions (2DV approximation) and the M2 internal tide amplitude from the 3D model provides an additional insight into analysing the model results.

The three sections emphasise the relationship between the intensification of the surface velocity by 46.5°N, 7°W (see Fig. 3) and the internal tide energy coming from the deep ocean.

For vertical sections S1 and S2 (Figs. 6 and 7), three-dimensional interactions are weak at points close to generation areas: the internal tide amplitude roughly follows the lines of 2D analytical beams. A first beam crosses point PF1 in deep layers between 1500 m and 2500 m where the M2 internal tide amplitude has maximum values. After reflection on the bottom depth, this beam coming from the French generation area crosses point PF3 at 1000 m on sections S1 and S2. However, in section S4, interactions between beams can be observed in the vertical distribution of the IT amplitude (see the two red lines plotted by 350 km from the Spanish slope as an example of beam trajectories, Fig. 8). The two spots of maximum IT amplitude modelled close to the French continental slope are generated by ray paths propagated in different vertical planes, and then reflected on the

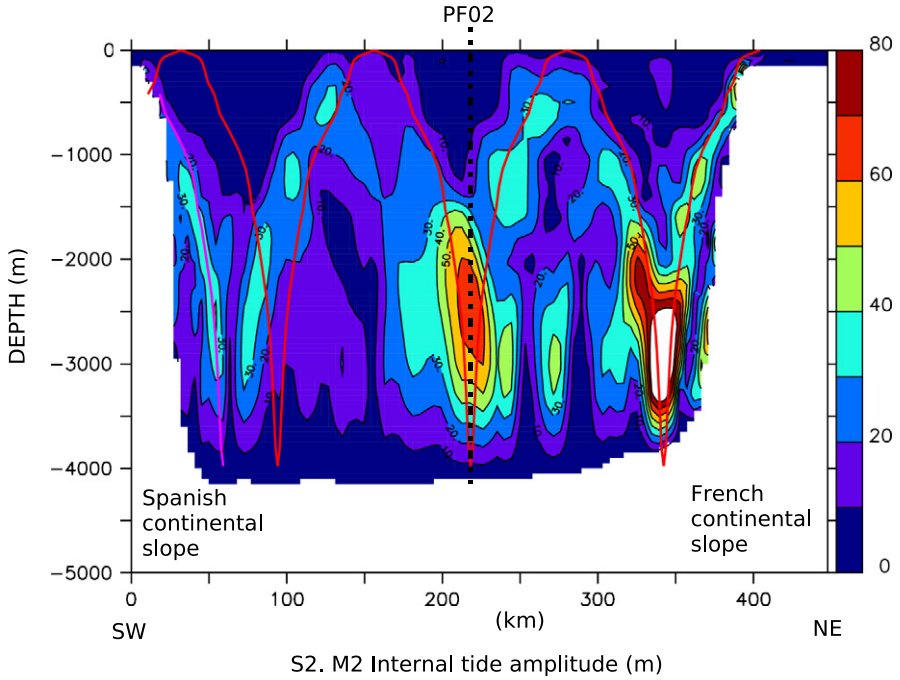

Fig. 7. Section S2. M2 internal tide amplitude (m), from SCHEM–HYCOM. In red, 2D analytical beam coming from the French shelf break (on the right). In pink, 2D analytical beam reflected on the Spanish shelf break (on the left). At PF2, internal tide has maximum value at 2500 m as on section S1.

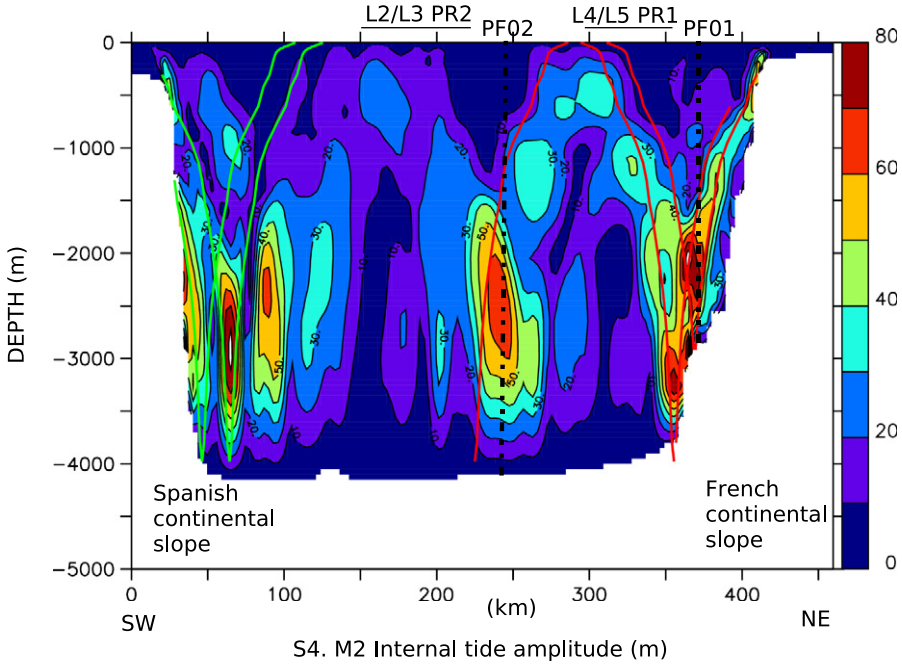

Fig. 8. Section S4. Internal tide amplitude (m), from SCHEM–HYCOM. In green, 2D analytical beams at 500 m and 1500 m showing different spots of generation over Spanish bottom slope (on the left). In red, 2D analytical beam coming from the French shelf break (on the right). On the French continental slope, the characteristics, reflected at different points on the bottom slope, produces a "defocusing" of the energy.

bottom slope at different locations (3000 m and 4000 m, Fig. 8). These multiple reflections on the bottom depth then produce a dispersion of IT energy and a widening of the IT beam in the deep ocean. In this section and close to point PF1, the M2 internal tide amplitude has maximum values between 2000 m and 3000 m.

Over the abyssal plain, the three vertical sections (Figs. 6 to 8) exhibit an internal tide amplitude maximum at 2500 m around PF2. This local maximum cannot be explained by a two-dimensional theory. Instead, this high internal tide amplitude is produced by the interaction of several ray paths coming from different generation areas as described in Section 3.2: PF2 is a point of positive interference between different IT beams coming from the French shelf break, between 46.8°N and 47.8°N, where the continental slope does not have the same geographic orientation (i.e. the angle from the North).

Other three-dimensional effects, which have an influence on the increasing internal tide energy in the central Bay of Biscay, are the reflection of the "French" deep ocean IT over the Spanish slope and the generation of local "Spanish" deep internal waves. As seen above, section S2 starts at the edge of the Spanish slope generation area (Fig. 4b). The IT amplitude distribution, modelled during the transient state, shows that the local generation is weak along this section. On the contrary, the strong French incident IT (beam in red) is reflected exactly at the Spanish shelf break, where the topographic gradient equals the beam slope (Fig. 7). Indeed, the distance between the French and Spanish continental slopes is resonant with the wavelength of the first deep ocean mode. The different beam lines (red and pink in Fig. 7) are plotted as an example of IT propagation. Even if they cannot represent all the three-dimensional IT distribution (as seen in the model result), these beam trajectories help to distinguish the reflected "French" IT (represented by the beam in pink), from the incident "French" IT (which follows the beam in red). The influence of this reflected wave is well observed over the first 150 km from the Spanish slope, with a maximum amplitude value of 40 m near the surface, 130 km from the Spanish continental shelf. Far away from the Spanish slope (between 150 and 200 km i.e. close to point PF2), the incident and reflected French waves faintly interact together as described in Section 3.2. The internal tide amplitude at point PF2 is mainly produced by interactions between "French" incident waves and then faintly reinforced by reflected waves.

The southern parts of sections S1 and S4 (Figs. 6 and 8) cross the second generation area along the Spanish slope, as shown on the body force distribution (Fig. 4a, b). Along these sections, therefore, there is a combination of waves generated over the Spanish continental slope (in green in Figs. 6 and 8) and "French" reflected waves. As seen in the vertical plane of the sections, the interaction of these two groups of waves generates an IT amplitude of 40 to 50 m between depths of 2000 m and 3000 m, which decreases (less than 30 m) after the first 100 km from the Spanish slope (Figs. 6 and 8). Therefore, one can assume that the region PR2 (Fig. 1) in the southern part of the Bay, will be affected by the different groups of waves.

3.4. Evidence of internal tides in the deep ocean

The model results and the in situ observations are now analysed at the three fixed points (black square in Fig. 3). PF2 and PF3 are on both sides of the central area of the Bay of Biscay, where the surface velocity reaches maximum values (see the area around 46.5°N–7°W, Fig. 3). PF1 is at the base of the continental slope at a depth of 3000 m.

3.4.1. Vertical motion

The evolution of the depth of the different isopycnic levels is a signature of the vertical motion produced by internal tide propagation. To quantify this vertical motion, the vertical deviation of each isopycne (compared to its averaged depth over two M2 tidal cycles), is computed from the observed density profiles (by using the density anomaly σ_{2000}) and from the model results. The time evolution of this vertical anomaly is displayed in Fig. 9 for the three points, PF1 to PF3.

The two models, REAL–HYCOM and SCHEM–HYCOM, correctly represent the semi-diurnal variations at the three points, with an internal tide phase clearly concordant with the data.

At point PF1, the amplitude of the internal tide has maximum values in the deep layers, between 1500 m and 2800 m, both in the data and in the two model results. The amplitude of the internal tide is higher at PF1 (80 m) than at PF3 (40 m). It is consistent with the

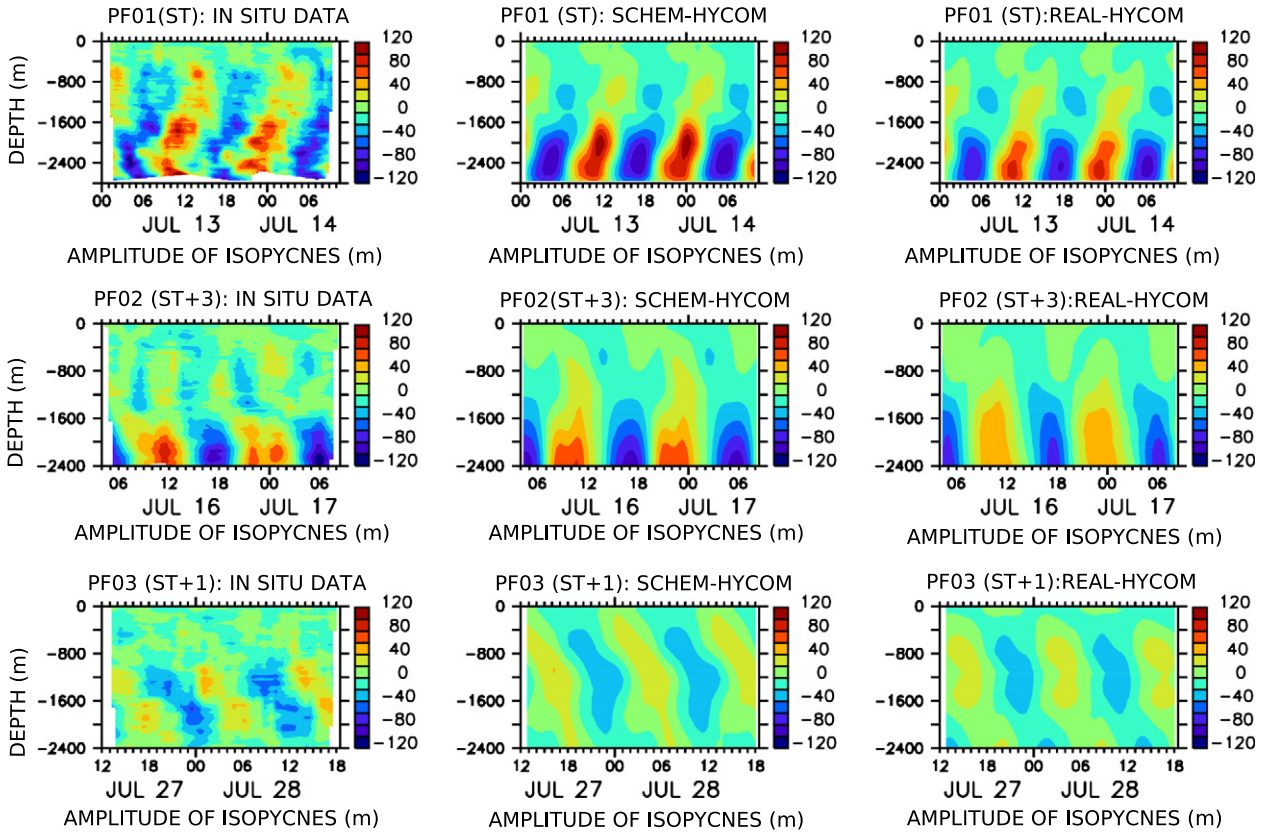

Fig. 9. Vertical anomaly of each isopycnic level, compared to its depth averaged, at PF1 (top), PF2 (centre), PF3 (bottom). In situ data (left), SCHEM–HYCOM (middle) and REAL–HYCOM (right). Data was collected at the spring barotropic tide (ST) at PF1, three days after at PF2 (ST + 3), one day after at PF3 (ST + 1). The modelled semi-diurnal variations are in phase with the data. IT maximums are well modelled on the vertical (excepted at PF3) and are explained by the propagation in the deep ocean. High vertical motion is revealed at PF2 by 2500 m in the central Bay.

variation of the tidal coefficient during the observations. At PF2, the vertical motion is at its highest at mid-depth (2500 m). Its magnitude is similar to PF1. The data at PF2 were collected two days after PF1 and the spring internal tide had the time to be propagated between the two points. Moreover, the strong vertical motion at PF2, twice as much as at PF3, both in the model and in the observations, is explained by the three-dimensional interactions highlighted in Sections 3.2 and 3.3. In the two models, the evolution of the vertical motion clearly concords with the observations at the two points PF1 and PF2. This is not the case at PF3, where the vertical motion's maximum is not observed at the same depth in the model (1200 m) and in the data (1600 m). This difference could be related to the mean vertical stratification. The mean density field defines the slope of the beams and therefore the vertical position of the internal tide. A bias could be produced by a low vertical resolution around the Mediterranean seawater mass (the model layers have a 200 m thickness in the deep ocean, see Section 2.2) in addition with an imperfect modelling of this water mass (the REAL–HYCOM uses initial conditions from the Mercator model where the Mediterranean water is not correctly positioned on the vertical).

The HYCOM model correctly reproduces the vertical phase lag for the three points. In particular, this difference is in opposition at points PF1 and PF3. At PF1, the deep layers are in advance compared to the upper layers, whereas at PF3 the deep layers lag behind the upper layers. This difference between the two points is consistent with a propagation of the internal tide across the two downward and upward energetic beams seen in sections S1 to S4 (Figs. 6 to 8). At point PF2, the evolution is dominated by the three-dimensional interactions and there is no difference in phase on the vertical.

The main difference between the two modelled solutions at the three points is that the internal tide in the SCHEM–HYCOM model is higher than the internal tide in the REAL–HYCOM model. In fact, a hybrid coordinate is used in the REAL–HYCOM case. This vertical coordinate can introduce dissipative effects in the upper layers, in particular close to the shelf break where the internal tide is generated. However, the solutions remain close, with a vertical motion magnitude clearly concordant with the data, and do not appear to be very sensitive to the meso-scale or large scale variability present in the REAL–HYCOM configuration.

3.4.2. Horizontal velocity

The horizontal velocity observed at the three fixed points is extracted from the LADCP stations and then compared to the model results.

The North–south component V, at the three locations is split in two parts: a time-average profile over two M2 tidal cycles (VMEANT), and the difference from this average (V–VMEANT) named the 'tidal component' (Fig. 10). This 'tidal component' can reach large values of 0.25 $m.s^{-1}$ near the bottom depth by 2500 m at point PF1 and near the surface layers at point PF2 (see Fig. 10b). The strong tidal current in the deep ocean is produced by the internal tide propagation. The SCHEM and REAL–HYCOM models reproduce the observations fairly well in terms of temporal and vertical variability. The stronger differences occur at PF2. Note that at this point, a time-average Northward current of 0.30 $m.s^{-1}$ (Fig. 10a), of the same order of magnitude as the tidal current, is measured over the first thousand metres. The drifting buoys C5 and C6, launched just after July 17th from an area close to PF2, also drifted northward. From July 17th to July 30th their drift was correlated with a large eddy in the centre of the Bay of Biscay, observed on an image of the surface chlorophyll concentration (Fig. 11). This current, associated with a particular meso-scale vortex, is not reproduced by the REAL–HYCOM model, and locally modifies the stratification and dynamics near PF2, which can explain the differences between the observations and model results.

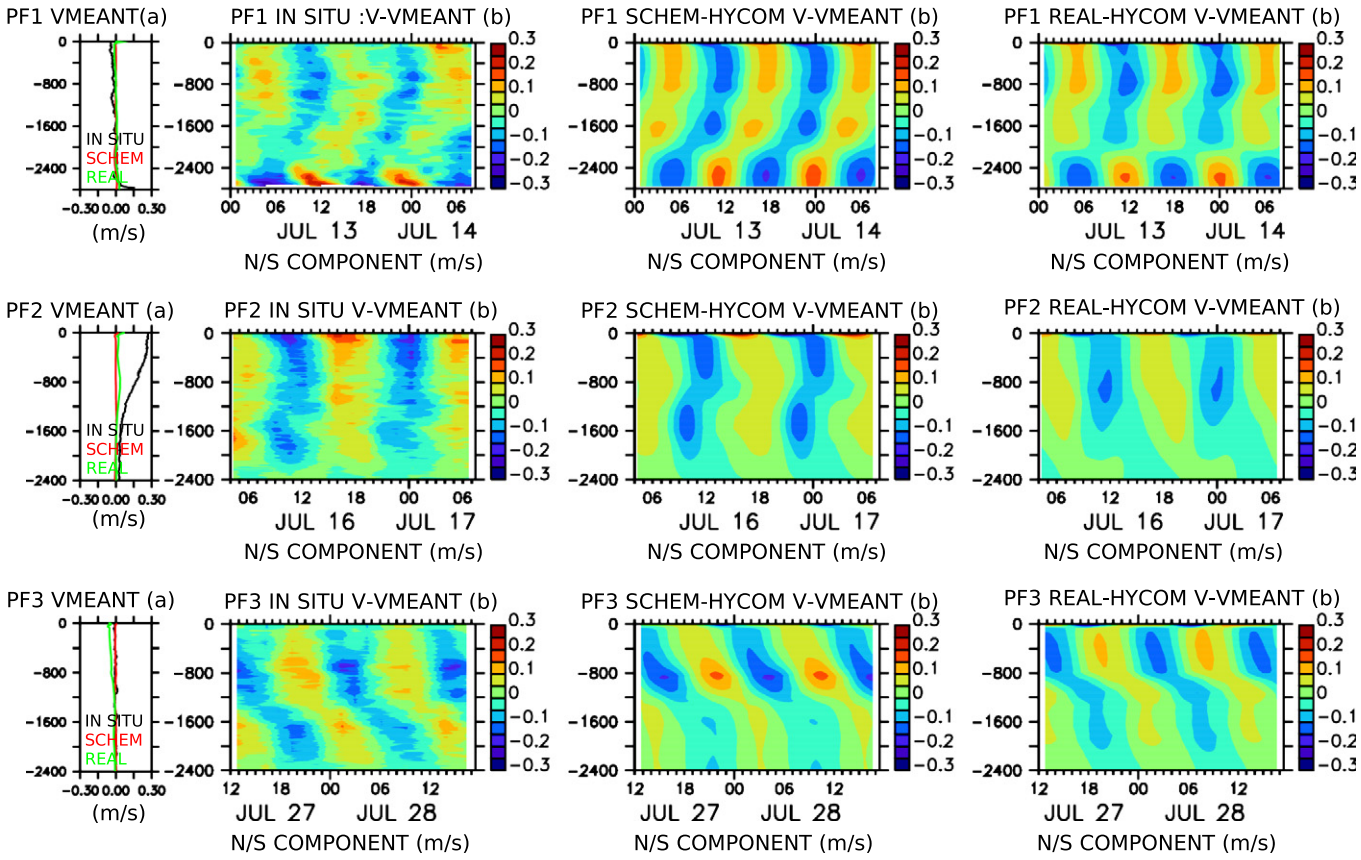

Fig. 10. North–south component V, split in a time-averaged on two M2 tidal cycles, Vmeant (a), and the deviation from Vmeant, V–Vmeant (b), at PF1 (top), PF2 (centre), PF3 (bottom). In situ data (left), SCHEM–HYCOM (middle) and REAL–HYCOM (right). The internal tidal velocity, V–Vmeant, reaches 0.25 m/s near the bottom depth by 2500 m at point PF1 and between 0 and 1000 m at point PF2. The SCHEM–HYCOM model fairly well reproduces the observations in the temporal and vertical variability at PF1 and PF3. At PF2, Vmeant = 0.3 m.s^{-1} is as high as the tidal current, V–Vmeant, measured over the first thousand metres. Vmeant is not reproduced by the model.

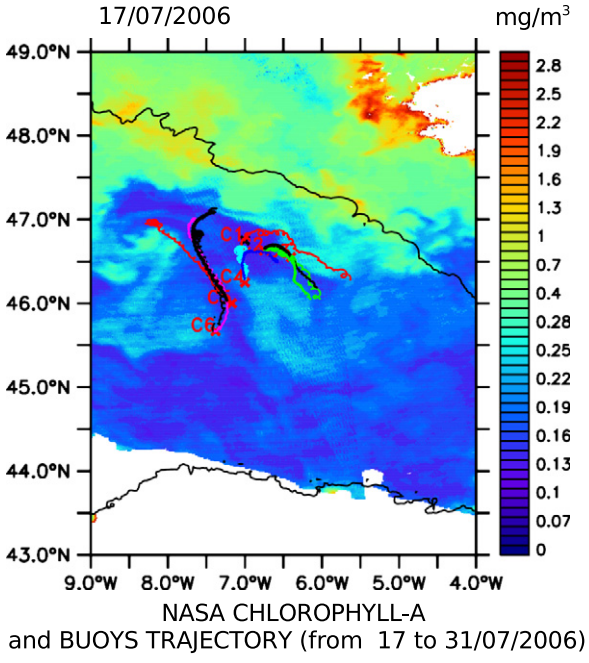

Fig. 11. Drifting buoys drogued at 15 m and 75 m were launched at the C1 to C6 locations on July 17, 2006. Their trajectories from July 17 to 31, 2006 are correlated with the eddy in the centre of the Bay of Biscay observed on the surface chlorophyll A distribution on July 17, 2006.

3.5. Evidence of outcropping beams

The model's ability to reproduce the internal tide structure along the deep ocean beams is now evaluated. The velocity field is described along VMADCP sections in the Northern region PR1.

Velocity data were collected along sections L2 (Fig. 12) and L4 (Fig. 13) of the PR1 region, during the barotropic spring tide, on July 14 and 15. The data of both VMADCP profilers (38 kHz and 150 kHz) were gathered to yield a vertical profile of the horizontal velocity from the sea surface down to 1200 m. The in situ observations are compared with SCHEM–HYCOM and REAL–HYCOM circulation along sections L2 (Fig. 12) and L4 (Fig. 13). In a thin layer close to the sea surface, the modelled velocity shows spatial variations which cannot be compared with the observations: the smoothing applied on the data (Hanning window on three points) associated with the vertical resolution of the VMADCP profilers (8 m and 24 m) induces a blind surface layer of 25 m. As described in Section 2.2, the model outputs are extracted at the positions x(t) of the measurements, to achieve a spatial distribution of the velocity at the time of the observations, U(x(t),z).

With the SCHEM–HYCOM results, the effect of the internal tide propagation on the velocity field can be analysed without any interactions with other processes. In both sections, the model shows a spatial evolution of the North–south component with vertical variation of the current concordant with the observations. Moreover, the slope of the analytical beams (in black on the plots) is very close to the positions of maximum velocity shear. The phase differences on the vertical, and the spatial distributions of the velocity modelled in the SCHEM–HYCOM case are very similar to the observations. The increase of the surface current, in the southern part of the sections, is

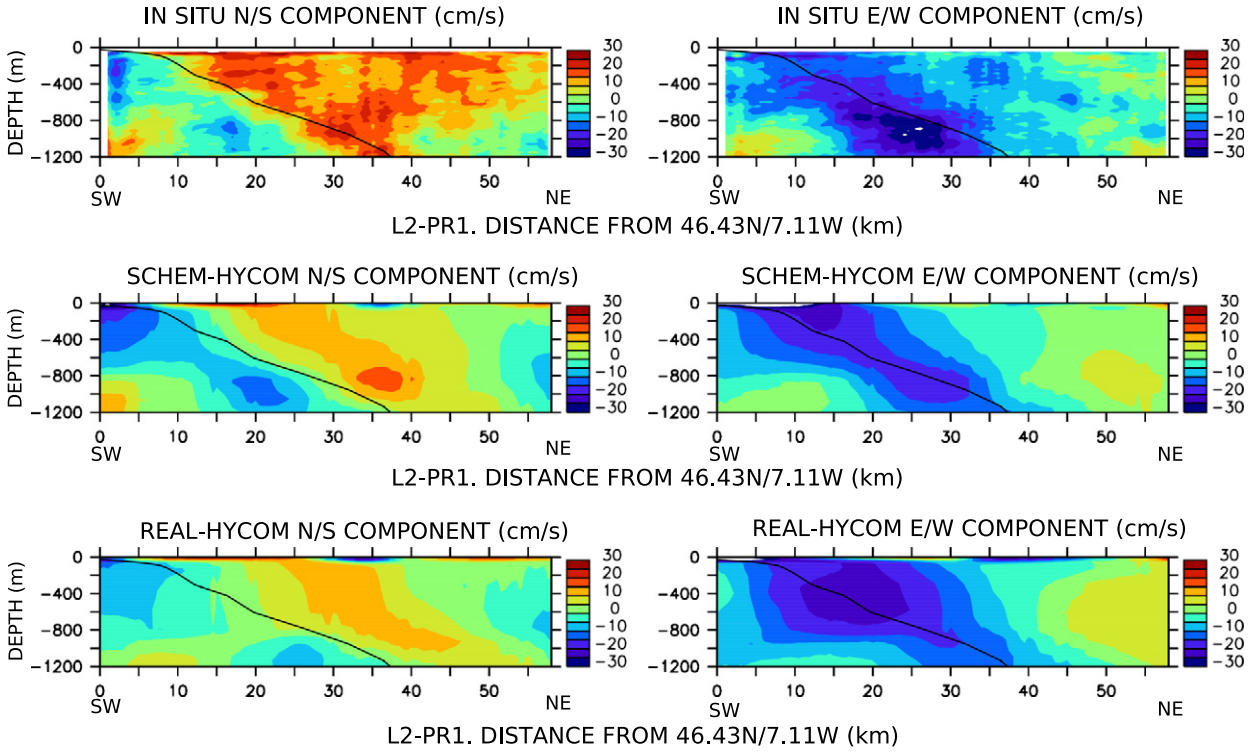

Fig. 12. Section L2 of the PR1 region at spring tide on July 14, 2006 (from Southwest, SW to Northeast, NE). N/S (left) and E/W (right) components. In situ data (top), SCHEM–HYCOM (middle) and REAL–HYCOM (bottom). Modelled velocity concords with the observations. Its vertical distribution is related to the slope of the characteristic (in black). The increase of the surface E/W current in the south part of the section, modelled by SCHEM–HYCOM, is related to the propagation of the internal tide energy along the upward beam. The modelled E/W velocity in REAL–HYCOM reaches more than 20 cm/s over the first 800 m, as in the observations.

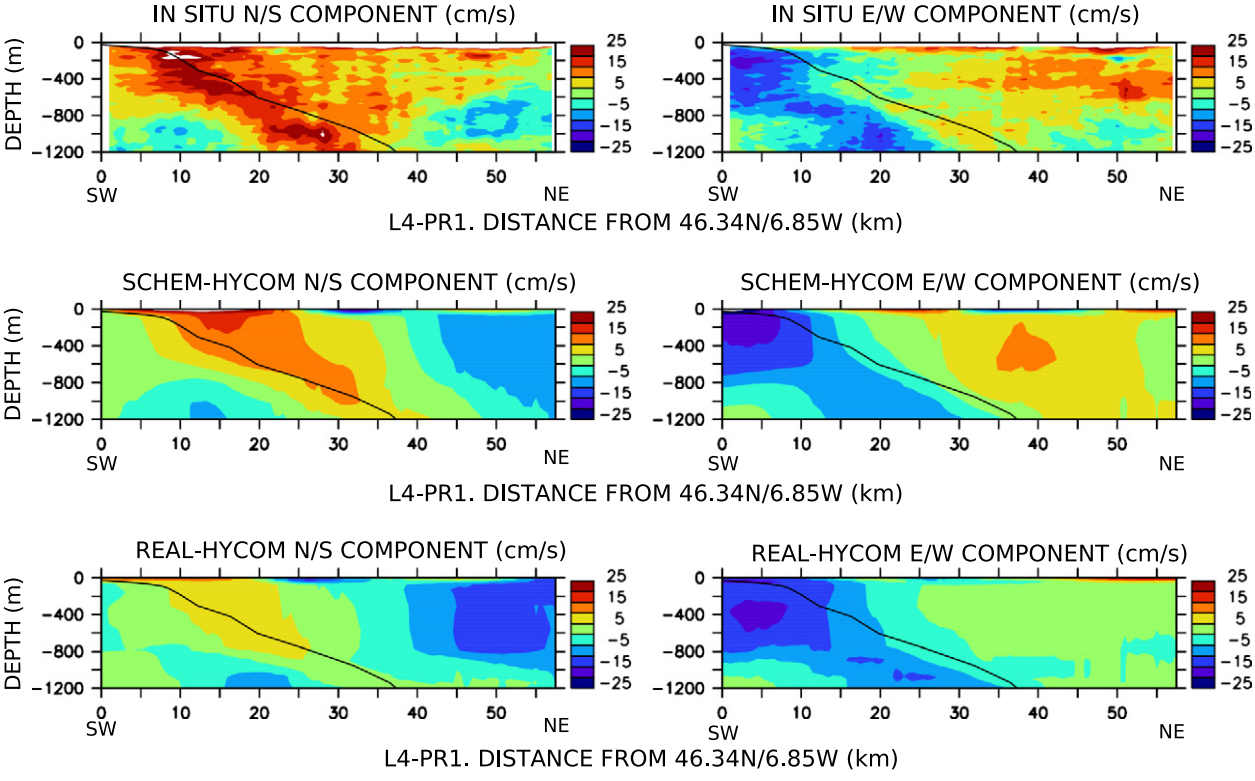

Fig. 13. Section L4 of the PR1 region. N/S (left) and E/W (right) components (from Southwest, SW to Northeast, NE). In situ data (top), SCHEM–HYCOM (middle) and REAL–HYCOM (bottom). Same result as in Fig. 12. The maximum of the E/W velocity, focussed in the surface layers between 0 and 800 m, is a signature of the outcropping region situated in the southern part of the section L4.

therefore related to the propagation of the internal tide across the upward beam.

As seen from the consistency between the observations and the SCHEM–HYCOM results, in the first one thousand metres, a large part of the circulation pattern can be explained by the internal tide velocity in the PR1 region (even though the data were collected when a northward meso-scale circulation was measured). The vertical anomaly of current speed, produced by the difference in phase across the beam can reach ± 0.15 m.s^{-1}.

On the two sections (Figs. 12 and 13), the outcropping region is situated in the southern edge of the PR1 region, with a maximum of the E/W component focussed in the surface layers between 0 and 800 m. Along section L2 (Fig. 12), the modelled E/W current magnitude in the REAL–HYCOM version is similar to the observations, with a value of more than 0.20 m.s^{-1} in the upper part of the profiles. The velocity of the internal tide in the deep ocean layers is well observed and reproduced by the models.

However, on section L2 (Fig. 12), the maximum value of currents along the beam, is not exactly at the same depth in the observations and in the two models. In addition, the position of the outcropping region near the sea surface differs from 5 to 10 km between the two models. This result can be correlated with differences between models and observations, already noticed at the point PF3. In the southern part of the PR1 region, i.e. around the first outcropping area, all the spatial and vertical variations of the mean density field are not accurately reproduced by the model (bad positioning of the Mediterranean water in particular). This results in a weak gap in the positions of the internal tides beams, which can generate the observed differences in the vertical distribution of the internal tide velocity.

In conclusion, the observations in the PR1 region have directly shown the presence of an upward beam of internal tidal energy striking the thermocline, in the central Bay of Biscay. And the effect of the deep ocean IT on the velocity structure in the first 1000 m is well reproduced by the HYCOM model.

3.6. Interactions of the deep ocean beams with the thermocline

Near the PR2 region, from 45°N to 46°N, 7.5°W to 8.5°W, the surface velocity field is amplified (Fig. 3), as waves coming from the French and Spanish shelf breaks interact constructively (Section 3.2). The linear interactions can be separated from non-linear effects by the analysis of the model results at different tidal frequencies.

In the surface layers (level depth 50 m), the spatial distribution of the M2 IT amplitude extracted from the SCHEM–HYCOM model, Fig. 14a, shows high IT amplitude along the main line of propagation described in Section 3.2 (A line in Fig. 5). Especially close to the PR2 region, this amplitude is increased by linear interactions between deep ocean waves ("French" incident and reflected ITs and Spanish ITs) and the interfacial IT in the seasonal thermocline: at the level depth of 50 m, along the main line A (Fig. 14a), a spatial variation of the IT amplitude is observed every half wavelength (25 km see Table 2) of the interfacial mode. The distribution of the M2 IT phase (Fig. 14b) at 50 m also provides information on these linear interactions. The variations of phase (every 50 km, i.e. at the wavelength of the interfacial mode over the plain see Table 2), show a wave mainly propagating from Northeast to Southwest (French incident IT) up to the PR2 region. Around this latter region, the reflected ITs slightly modify the phase distribution. Along the SAR line direction (line B Fig. 14a) the phase distribution shows evidence of reflected ITs propagated north-westward (Fig. 14b). Moreover, this phase distribution clearly underlines the activity region of every group of IT waves (Spanish waves and French incident and reflected waves) with interactions between them from the Spanish continental slope up to 45.5°N.

The PR2 region is also an area where non-linear effects are increased by interactions between the interfacial mode and the deep ocean IT waves when they outcrop the surface layers. These nonlinear

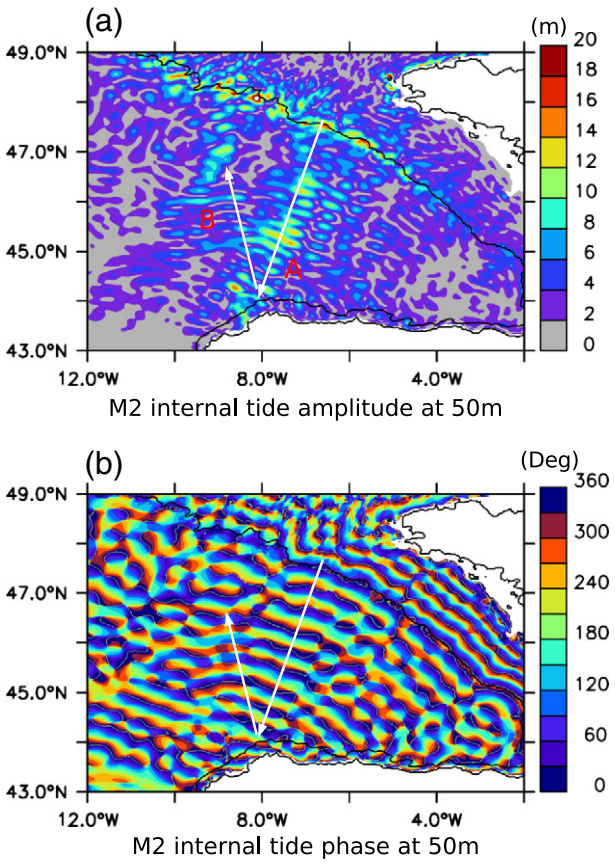

Fig. 14. M2 internal tide amplitude (a) and phase (b) at level depth 50 m, extracted from SCHEM–HYCOM model. Lines in white: axes where internal tides interact together. Arrow (A): the spatial variation of the IT amplitude every half wavelength (25 km) of the interfacial mode denotes linear interactions between incident and reflected ITs. The variations of phase (every 50 km, i.e. at the wavelength of the interfacial mode), show the great influence of the French incident wave with a propagation direction mainly from Northeast to Southwest up to the PR2 region. Along the SAR line direction (arrow B) the phase distribution shows evidence of reflected ITs propagated north-westward.

interactions are shown by the modelled IT at the harmonic frequencies M4 and MS4: the sum of the M4 and MS4 IT amplitude near the surface (at 50 m) and the phase of the M4 IT are extracted by Fourier analysis from the SCHEM–HYCOM model, forced by the four semi-diurnal tidal waves (Fig. 15). The M4 + MS4 amplitude reaches 6 m around the PR2 region (Fig. 15a). This amplitude is not negligible compared to the M2 amplitude in the same region (16 m, Fig. 14a). Moreover, the non-linear interactions between deep ocean waves and interfacial IT around the PR1 and PR2 regions are demonstrated by increasing of M4 + MS4 amplitude in these areas (Fig. 15a). The spatial extension of these nonlinear effects is reinforced in the PR2 region (compared to the PR1 region) by the interactions between the incident and reflected ITs.

In the PR2 region, the M4 + MS4 IT amplitude has spatial variations which follow half the wavelength of the different modes corresponding to IT frequencies (for the deep ocean modes 2 and the interfacial mode $\lambda_{m4}/2$ are close to 9 km, see Tables 1 and 2). The spatial distribution of these harmonics, characteristic of non-linear interactions, again shows that the French reflected IT and the Spanish IT have a high influence in the PR2 region but not in the PR1 region: in this last case no variation of amplitude (at $\lambda/2$) characteristic of stationary waves is modelled.

In the deep ocean, outside the main lines of linear interactions between waves (lines A and B Fig. 15), the spatial distribution of the M4 phase in the surface layer (Fig. 15b) varies at a wavelength of nearly 18 km (i.e. deep ocean mode 2 or interfacial mode wavelength,

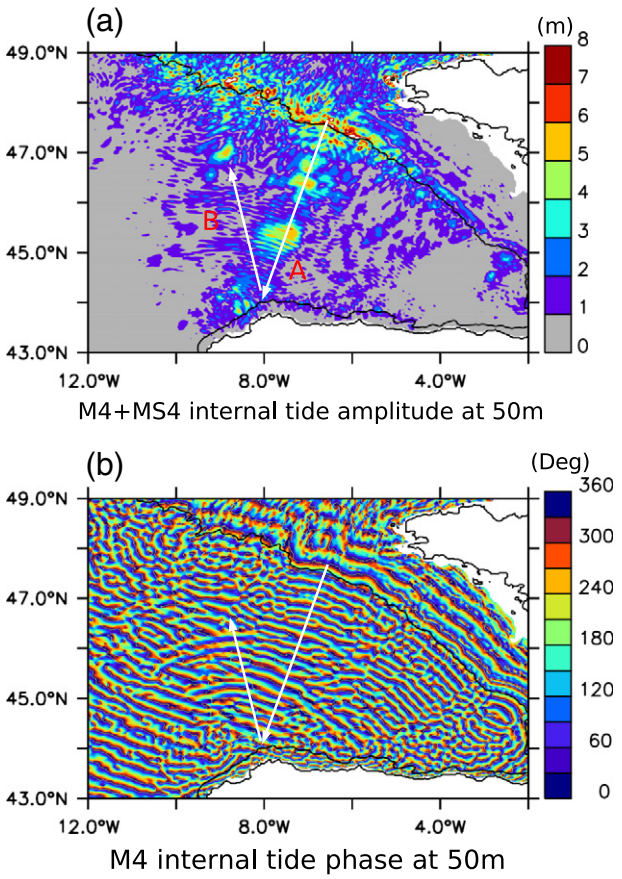

Fig. 15. M4 + MS4 internal tide amplitude (a) and M4 phase (b) at level depth 50 m, extracted from SCHEM–HYCOM model. (a): the non-linear interactions between deep ocean waves and interfacial IT are demonstrated around the PR1 and PR2 regions by increasing the M4 + MS4 amplitude. The spatial extension of these nonlinear effects is reinforced in the PR2 region (compared to the PR1 region) by the interactions between the incident and reflected IT waves: in the PR2 region, the M4 + MS4 IT amplitude has spatial variations (~10 km) which follow half the wavelength of the different modes corresponding to IT frequencies. By 45°N 8.5°W, the M4 phase distribution shows the direction of propagation of the incident (line A) and reflected waves (line B) with successive red–blue lines in opposite direction.

see Tables 1 and 2). By 45°N 8.5°W, close to the PR2 region, the M4 phase distribution clearly shows the direction of propagation of the incident (line A) and reflected waves (line B) with successive red–blue lines in opposite direction.

3.7. Internal waves at high frequency

To underline non-linear interactions between the interfacial wave and the deep ocean IT, the two sections L2 and L3 of the PR2 region, are now described.

In these sections, the velocity data of the two VMADCP are gathered. An in situ "baroclinic" velocity is defined as the deviation from the depth-averaged velocity measured over the first thousand metres. A Northward depth-averaged current of 0.25 $m.s^{-1}$ is measured in the north-eastern part of the section L2 (Fig. 16c bottom). This current can be related to the same meso-scale feature observed at point PF2 (see the tidal-averaged velocity in Fig. 10) which is at the end of section L2: the observed depth-averaged current between 0 and 1000 m can be associated with the meso-scale circulation not negligible in the northern part of the PR2 region. On the other hand, the in situ "baroclinic" velocity is assumed to be associated with the IT propagation: the meso-scale circulation also has a baroclinic component, negligible in the first 200 m in comparison with the internal tide signature (at point PF2, close to the PR2 sections, the tidal-averaged current is homogeneous in the first 200 m).

On section L2, the distribution of the in situ temperature is compared to the SCHEM–HYCOM results (Fig. 16a and b). As described in Section 2.2, the model outputs are extracted at the positions x(t) of the measurements, to achieve a spatial distribution of the temperature at the time of the observations, T(x(t),z). Vertical variations of the thermocline are measured between 35 km and 45 km from the starting point of the section (see Fig. 16a). The SCHEM–HYCOM model well represents this deepening at the same location as in the observations (Fig. 16b). The vertical variations of temperature measured from 35 km to 45 km are therefore related to the propagation of the IT in the seasonal thermocline (since the SCHEM–HYCOM model runs with tidal forcing only). This modelled IT, exactly in phase with the observations, shows the model's ability to take into account the three dimensional propagation of internal waves, even if the model does not represent the small scales horizontal variability (the comparison between the model results and the observations shows the limitation of a hydrostatic model, which cannot represent the high non-linear structures even if the horizontal resolution is increased).

In the first 300 m, the deepening of the thermocline generates a vertical variation of the observed "baroclinic" velocity which reaches nearly 0.40 $m.s^{-1}$ (Fig. 16c). The position of this vertical variation along the section L2 is correlated with the outcropping of a deep ocean upward beam (Fig. 16d): the SCHEM–HYCOM velocity varies from 0.10 $m.s^{-1}$ to 0.25 $m.s^{-1}$ between 0 and 1000 m, at 35/45 km from the starting point of the section. Small-scale variability observed in the thermocline depth is associated with vertical variations of currents. These spatial oscillations generated in the outcropping region, can be related to the spatial distribution of the internal tide amplitude modelled in the PR2 region where non-linear interactions are reinforced (see IT amplitude of M4 + MS4 Fig. 15a). In section L3 (Fig. 17) the vertical variation of the current, due to the deepening of the thermocline is not as high as in L2, but is also related to the deep ocean IT and associated baroclinic current. Again small-scale oscillations are observed in the thermocline, correlated with the modelled interfacial wave too.

In the observations (vertical sections L2 and L3), the spatial scales of the velocity and thermocline depth fluctuate from 2 km to 5 km, at a length scale close to those of ISW trains. Numerous analytical models developed under weakly non-linear and non-hydrostatic approximations described the characteristics of internal solitary wave trains (Apel et al., 2007). In the more simple case of a two layer ocean, under the KDV approximation, the phase celerity 'c' and the characteristic width, '1/q' of a solitary wave depend on its amplitude 'a' (Gerkema, 1996):

$$c = c_0 * \left[1 + a * \frac{(h_1 - h_2)}{2 * h_1 * h_2}\right], \tag{7}$$

$$\frac{1}{q} = \frac{4 * (h_1 * h_2)^2}{3 * (h_1 - h_2) * a}, \tag{8}$$

where $c_0 = g'.\frac{h_1 * h_2}{(h_1 + h_2)}$ is the linear IT phase speed, function of the reduced gravity g′ and the thickness of the upper (h_1) and lower (h_2) layers.

An ISW train in the seasonal thermocline is therefore characterised by a depression of high amplitude with narrow width '1/q', (if 'a' increases, 'c' increases and '1/q' decreases) followed by other successive depressions of weaker amplitude but larger width than the first one (in deep ocean the layer depth h_2 is much greater than h_1, and the solitons generate a depression of the thermocline rather than an elevation). Over the continental shelf, the soliton width has a typical length scale of 1 km, for a long wave speed $c_0 = 1$ $m.s^{-1}$ (as in the deep ocean in summer, see Table 2) and a depression of 15 m (Apel, 2002). Under rotation, and especially in the deep ocean where the layer depth h_2 increases, the length scale of the KDV-soliton is increased (Eq. (7)): numerical

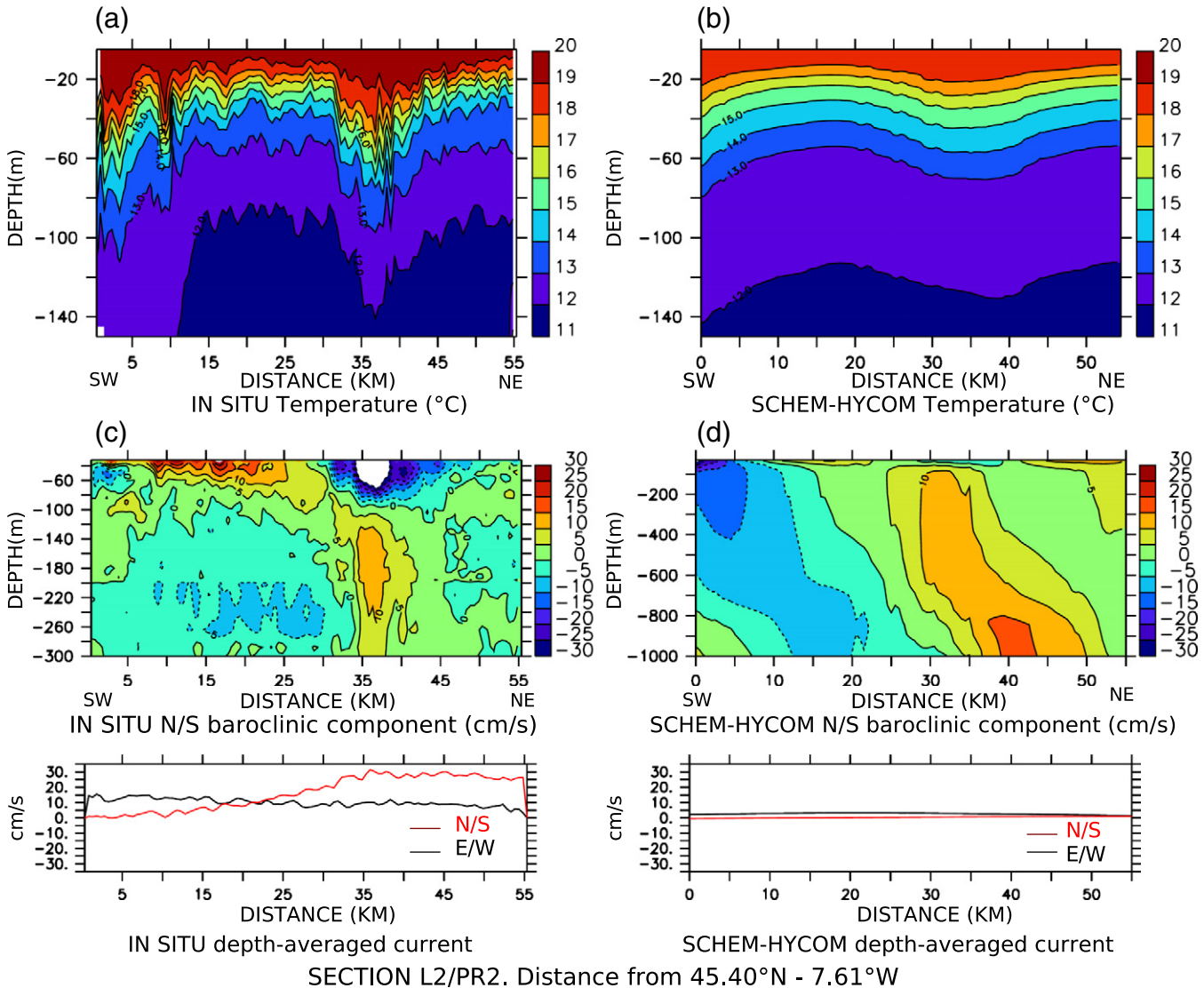

Fig. 16. Section L2 of the PR2 region. In situ data (left), SCHEM–HYCOM model (right). Vertical distribution of temperature from 0 to 150 m (a, b), and of N/S velocity (c, d). Velocity is split in a depth-averaged component (from 0 to 1000 m) $\overline{V}$, and a "baroclinic" component. On the observations (c bottom), $\overline{V}$ reaches 0.25 m.s^{-1} at the North-East edge of L2, as Vmeant at point PF2. The deepening of the observed thermocline (a) is in phase with the modelled interfacial internal tide (b). This deepening generates a vertical variation of the observed baroclinic velocity of nearly 40 cm/s (c), correlated with the outcropping of the deep ocean upward beam (d).

non-hydrostatic simulations, under typical summer stratification at the Bay of Biscay (Gerkema, 2001), reproduce solitary waves with wavelength of nearly ~2 km. But they are not ordered, as expected, by the two layer theory. The spatial scales, from 2 km to 5 km, observed along the sections L2 and L3 are slightly longer than the theoretical ISW wavelengths (1–2 km) but shorter than the modelled wavelengths produced by the non-linear interactions around PR2 region (Fig. 15, Tables 1 and 2). Therefore, the observations reproduce non-linear features at spatial scales close to the ISWs' characteristic length scales, however, the spatial resolution along the sections L2 and L3 is not fine enough to clearly observe solitary wave trains. There is a bias in the observed wavelengths that comes from the temperature collected at a variable spatial scale, function of the speed of the ship, ~ 8 knots, and the variable vertical speed of the SEASOAR ocean undulator (from 1 m/s to 2 m/s, Section 2.1). Within these parameters, the spatial resolution varies from 0.5 km to 1.5 km; this insufficient resolution does not measure the narrowest wavelengths of solitary waves.

Numerous and strong non-linear features are thus observed at the two in situ sections. Even though their spatial and time resolutions seem to be too large, they are likely to be associated with the generation of solitary waves during the deepening of the thermocline when the deep IT outcrops at the surface.

In the PR2 region, the REAL HYCOM solution has also been compared to the observations. In this last case the interfacial wave is not modelled as accurately as in the SCHEM–HYCOM case, the IT in the seasonal thermocline is not in phase with the observations. This bias is probably related to the modelled mean density field.

3.8. Effect of the mean density field on the internal tide evolution

The effect of the mixed layer evolution on the internal tide propagation will now be investigated. The temperature of REAL–HYCOM and SCHEM–HYCOM, is compared to the observations collected by the two drifting thermistors chains, deployed at C3 and C4 (Fig. 1). Chain 171 (point C4) measures high internal tide amplitude, between July 19 and 21(Fig. 18b). At this time, the chain is still located within the main energetic section, close to the region where the first "French" beam, reflected on the bottom depth outcrop the sea surface (see black points in Fig. 18a). After July 21, the chain drifts eastward, leaving the main internal tide region, and the surface

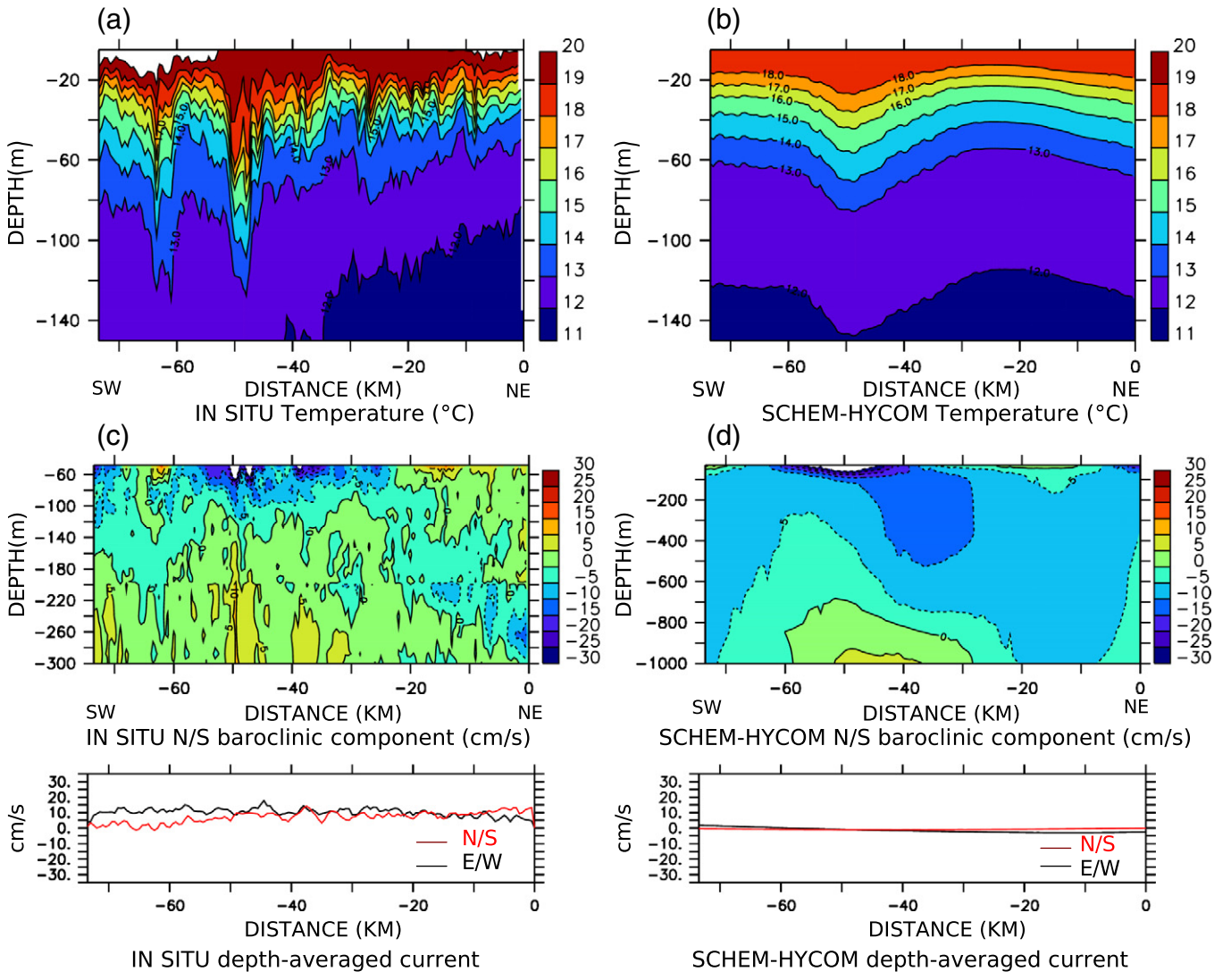

Fig. 17. Same as Fig. 16 for section L3 of the PR2 region. The vertical variation of current (b) due to the deepening of the thermocline (a) is not as high as on L2, but it is related to the deep ocean baroclinic current modelled by SCHEM–HYCOM too (d). The deepening of the thermocline is in phase with the modelled interfacial wave (b).

tide decreases (the barotropic neap tide is on July 21 and the baroclinic neap tide has a time lag of about one day along the buoy trajectory). The measured temperature does not show as high an internal tide as before. SCHEM and REAL HYCOM models clearly represent this feature with a higher internal tide in the first days than in the following (Fig. 18b). Moreover, the REAL–HYCOM model reproduces the heating of the surface layers (Fig. 18b) fairly well. If we take into account the duration of the simulation (six months from January without any data assimilation), this comparison proves the model's ability to reproduce the surface layers' evolution under atmospheric and tidal forcing. Another point of comparison can be found in the IT propagation, produced at the moment when the maximum value of the internal tide amplitude occurs: the SCHEM–HYCOM model and the observations are nearly in phase. However, the modelled IT with REAL–HYCOM has a delay of about one or two days with the observed IT. In this case, if the internal tide structure is clearly reproduced, the weak delay in the IT propagation can have a lot of origins, related to the modelled mean density field (position of the mixed layer depth, position of the Mediterranean water which has an influence on the internal tide beams' positions and consequently on the outcropping regions). In the SCHEM–HYCOM configuration, the mean density field is defined by an average of observations in July. Therefore the IT wavelengths are modelled precisely.

In August 2006, model results are compared to the observations along the trajectory of the 174 chain (point C3, Fig. 1). In one month, the chain drifted southeast and the buoy trajectory followed the edge of the baroclinic currents' maximum value (Fig. 19a). The REAL–HYCOM model clearly reproduces IT action on the surface baroclinic currents, with a spatial variation at the wavelength of the interfacial mode. Only the time evolution of the REAL–HYCOM temperature is compared to the observations along the buoy trajectory, Fig. 19b (the mean density field used in the SCHEM–HYCOM reproduces the stratification in July; therefore this model cannot be used in August since the warmth of the surface layers between July and August severely modify the baroclinic modes.) As in July, REAL–HYCOM model clearly reproduces spatial and time variations of the mixed layer temperature as well as evolutions in internal tides. The high baroclinic tide modelled on 16 August (Fig. 19b) is related to the trajectory of the buoy crossing locations, where high baroclinic surface currents occur at the same time (Fig. 19a). But this spring baroclinic tide is measured on 13 and 14 August (Fig. 19b). The delay between the model and observations could be related to the modelled mean vertical

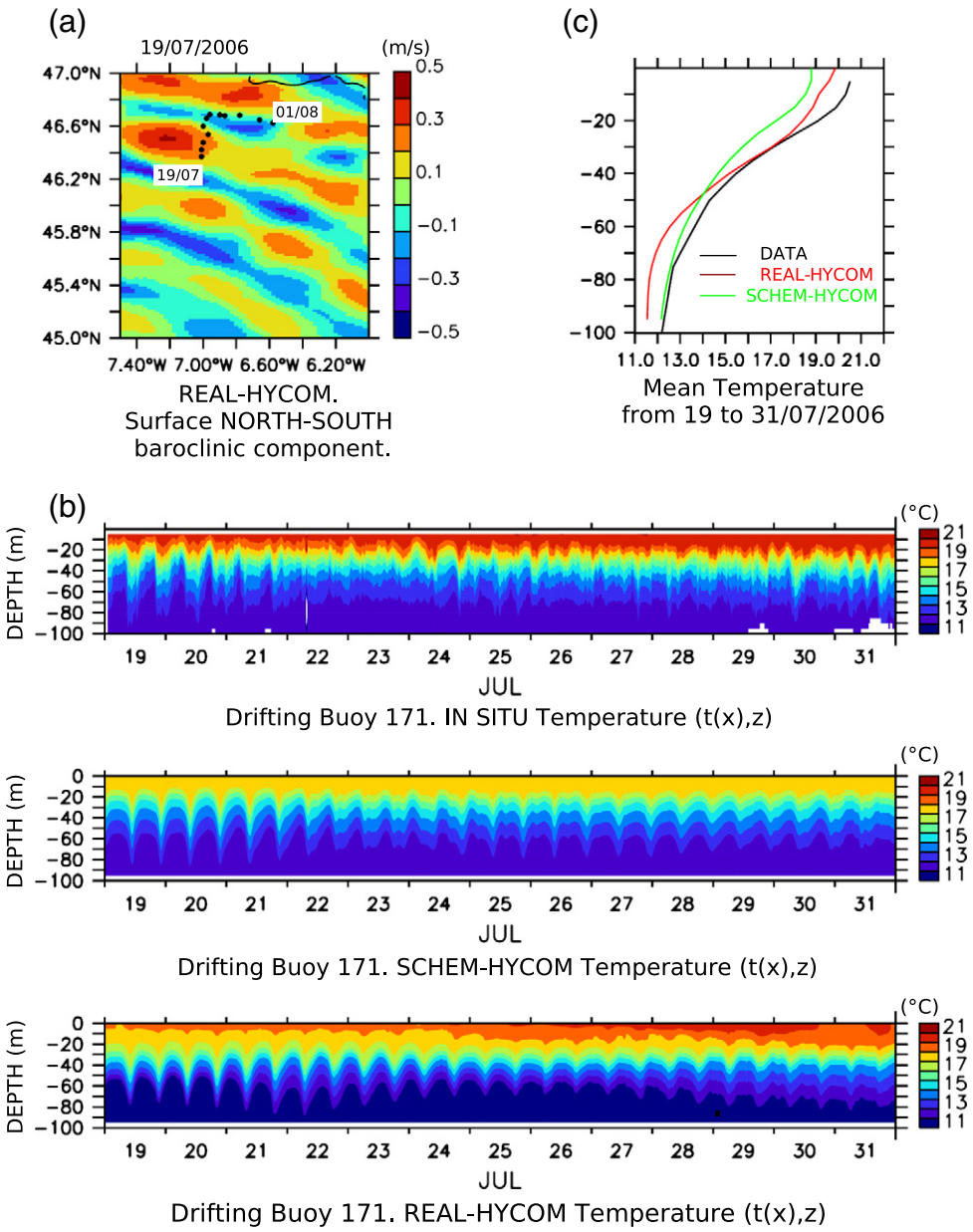

Fig. 18. Trajectory of the drifting chain 171 from July 19, to August 01, 2006 (a). In situ data and modelled time series (b). Time-averaged profile of temperature (c). High internal tide is measured and well modelled by SCHEM–HYCOM (b) between the July 19 and 21, when the chain is still along the energetic section and close to the outcropping of the deep ocean IT beam (a). The mean vertical stratification from 0 to 100 m of the REAL–HYCOM model shows a bias of 0.5 °C to 1 °C with the observations (c); this bias could modify the IT phase celerity and the instant when the IT reaches a maximum value in the REAL–HYCOM solution (b).

stratification from 0 to 100 m, which does not fully concord with observations: there is a bias on the modelled mixed layer depth, which is too deep compared to observations (Fig. 19c). This bias increases between July and August (Figs. 18c and 19c). These results suggest that the phase speed of the interfacial wave which depends on the mean stratification and on the mixed layer depth is not clearly modelled in the REAL–HYCOM case, and consequently, the propagation of the interfacial internal tide is modified. The link made between the bias on the mean vertical stratification and the differences in the data/model comparisons is only speculation. However, the trajectory of the buoy between, 12 and 16 August, follows the maximum edge of surface baroclinic currents (Fig. 19a), and a weak modification in the mean stratification could change the modelled IT in the thermocline. The modelling of the mean density field in the surface layers should be improved in the REAL–HYCOM simulation.

3.9. Modelling improvements

One bias of the REAL–HYCOM simulations is that the modelled mixed layer is slightly too deep in July and August 2006. This deepening can have an effect on the modelled internal tide inside the seasonal thermocline which could result in a time lag in the spring baroclinic event between the observations and the simulations. The REAL–HYCOM simulations, used here to interpret the observations in summer 2006, were obtained throughout the year 2006; the excessive deepening of the mixed layer is confirmed during autumn months. This problem can be addressed in two different ways.

First, the KPP model used in REAL–HYCOM, is sensitive to pure convection situations during the night (Jezequel et al., 2004). This particularity generates a deepening of the thermocline more effective than in TKE models. Perhaps this effect is reinforced in the simulations

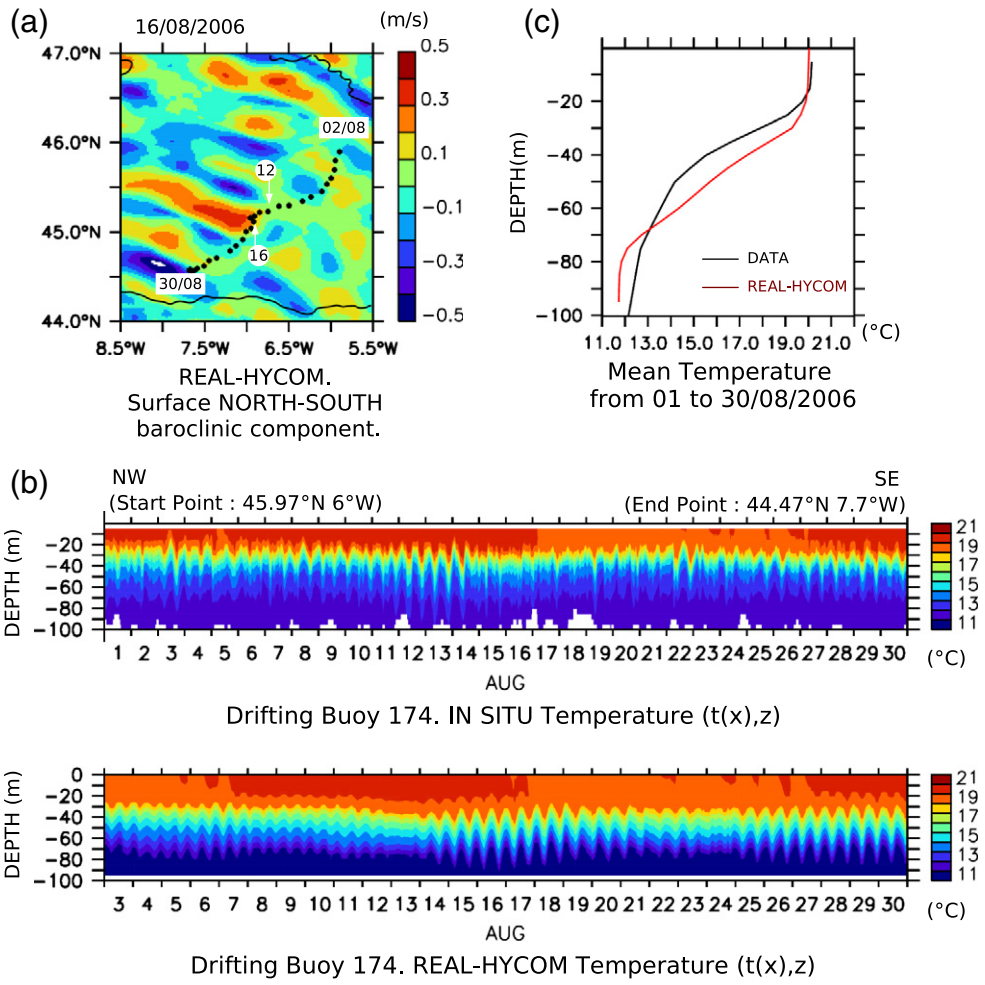

Fig. 19. Trajectory of the drifting chain 174 from 01 to 30 August (a). In situ data and modelled time series. Time-averaged profile of temperature in August 2006 (c). The spatial and time evolutions of the surface temperature are well reproduced by the model. High internal tide modelled by REAL–HYCOM (16–17 August) is in delay of about one or two days compared to the observations (b). The bias on the mean vertical temperature profile is increased (b) compared to the July situation. The modelled mixed layer depth is too deep for at least 10 m.

presented here, where atmospheric fluxes are introduced every 6 h. Perhaps the diurnal evolution of the thermal budget is not clearly represented by this time scale. However, the spatial variation of the atmospheric fluxes is introduced correctly into the model. The REAL–HYCOM model clearly reproduces the time and spatial variations of the surface temperature due to the atmospheric fluxes (Figs. 15b and 16b).

Second, a higher vertical resolution in the REAL–HYCOM, especially in the transition layers (hybrid layers), which are generally at the base of the MLD, may improve the representation of the vertical mixing. The KPP model is indeed sensitive to vertical resolution (Jezequel et al., 2004; Large et al., 1994; Renaudie et al., 2009). A vertical resolution of 5 m is necessary to represent the dynamics of the mixed layer. The thickness of the hybrid layers is generally higher than this threshold. An increase of the number of vertical layers may improve the solution.

Meso-scale circulation is another, maybe more difficult, process to reproduce to achieve more realistic results. In the area around 7°W 46.5°N, a northward current (time-averaged on the M2 tidal cycle) of 0.25 $m.s^{-1}$ was measured over the first 500 m at point PF2. This velocity is related to an eddy observed on chlorophyll imagery. This northward component was also measured along VMADCP sections in the south of PF2, and the different buoys launched at the same time drifted northward for ten days after these observations. The REAL–HYCOM outputs do not represent the meso-scale circulation in this area, which can modify the local IT dynamics or impair the interpretation of observations. There is still much work to do to reproduce a realistic, real-time, meso-scale circulation in models at a regional scale, and data assimilation is required.

Finally, basin or global scale models, such as the MERCATOR model, are generally used to initialize at the open boundaries. The large scale stratification (associated with the deep water mass distribution) and meso-scale feature structure and positioning still have to be more accurately represented in these models as they are also a major source of errors in the modelling of IT.

4. Conclusions

The survey conducted in July 2006 highlights the existence of deep ocean internal tides. In the spring baroclinic tide, the vertical motion measured in the deep ocean can reach 80 m by 2500 m at particular locations, and the baroclinic tidal current related to this internal tide reaches 0.30 $m.s^{-1}$ at the base of the continental slope and 0.25 $m.s^{-1}$ in the middle of the Bay of Biscay at 46°N/7.2°W. The HYCOM model clearly reproduces these internal tide structures with quantitative estimations concordant with observations.

Therefore, the use of the HYCOM model in different modes enabled the study of the three-dimensional interactions between the internal tide waves observed during the campaign at sea. This analysis revealed positive three-dimensional interactions around 46.5°N/7.2°W between internal waves coming from different generation spots over the French

shelf break. These interactions explained the observed intensification of the deep ocean internal tides at a depth of 2500 m around 46°N/7.2°W.

In addition, non-linear effects intensified by the interactions between the deep ocean IT and the surface layers were observed in the second outcropping region around 45.5°N/7.5°W. In this area, high frequency waves measured in the seasonal thermocline were related to the observed vertical shear of the current. The numerical simulations demonstrated the direct relationship between these features and the seasonal internal tide reinforced by the tidal current coming from the deep ocean.

The observed non-linear small scale features were therefore interpreted as ISW, generated by the deepening of the thermocline when the deep IT reaches and intensifies at the surface.

Through this work, a realistic HYCOM model was achieved and was used to simulate the mixed layer and the thermocline evolution, taking into account atmospheric fluxes and tidal forcing. The in situ observations and the drift of the different buoys, during the period of observation, covered wide sections of the Bay of Biscay and allowed some major events associated with IT propagation in this area to be confirmed. The imperfect three-dimensional modelling, since HYCOM still uses hydrostatic approximation and therefore cannot reproduce ISW, can thus be used to identify the areas of interest and to predict the evolution of ITs in this region.

References

Allen, J., Cornell, V., Moore, M., Crisp, N., Dunning, J., 2002. Operational oceanography using the 'new' SeaSoar ocean undulator. Sea Technol. 43 (4), 35–40.

Apel, J.R., 2002. Oceanic internal waves and solitons. An Atlas of Oceanic Internal Waves (May 2002) by Global Ocean Associates Prepared for Office of Naval Research — Code 322PO.

Apel, J.R., Ostrovsky, L.A., Stepanyants, Y.A., Lynch, J.F., 2007. Internal solitons in the ocean and their effect on underwater sound. J. Acoust. Soc. Am. 121 (2), 695–722.

Azevedo, A., DaSilva, J.C.B., New, A.L., 2006. On the generation and propagation of internal solitary waves in the southern Bay of Biscay. Deep-Sea Res. 53 (6), 927–941. doi:10.1016/j.dsr.2006.01.013.

Baines, P.G., 1982. On internal tide generation models. Deep Sea Res. Part A 29, 307–338.

Barnier, B., Madec, G., Penduff, T., Molines, J., Anne-Marie, Treguier, Le Sommer, J., Beckmann, A., Biastoch, A., Boning, C., Dengg, J., Derval, C., Durand, E., Gulev, S., Remy, E., Claude, Talandier, Sebastien, Theetten, Maltrud, M., Mcclean, J., De Cuevas, B., 2006. Impact of partial steps and momentum advection schemes in a global ocean circulation model at eddy-permitting resolution. Ocean Dyn. 56 (5–6), 543–567.

Bleck, R., 2002. An oceanic general circulation model framed in hybrid isopycnic–cartesian coordinates. Ocean Modell. 4, 55–88.

Da Silva, J.C.B., New, A.L., Azevedo, A., 2007. On the rôle of SAR for observing local generation of internal solitary waves off the Iberian Peninsula. Can. J. Remote Sens. 33 (5), 388–403.

Garrett, C., Gerkema, T., 2007. On the body-force term in internal-tide generation. J. Phys. Oceanogr. 37, 2172–2175.

Gerkema, T., 1996. A unified model for the generation and fission of internal tides in a rotating ocean. J. Mar. Res. 54 (3), 421–450.

Gerkema, T., 2001. Internal an interfacial tides: beam scattering and local generation of solitary waves. J. Mar. Res. 59, 227–255.

Gerkema, T., Lam, F.P.A., Maas, L.R.M., 2004. Internal tides in the Bay of Biscay: conversion rates and seasonal effects. Deep-Sea Res. 51, 2995–3008.

Holloway, P.E., 2001. A regional model of the semi-diurnal internal tide on the Australian North West Shelf. J. Geophys. Res. 106, 19,625–19,638.

Jezequel, N., Mazé, R., Pichon, A., 2002. Interaction of a semi-diurnal tide with a continental slope in a continuously stratified ocean. Deep-Sea Res. 49, 707–734.

Jezequel, N., Pichon, A., Maze, R., 2004. Influence of convection on mixed-layer evolution: comparison of two mixing parameterizations with buoy data in the Bay of Biscay. J. Mar. Syst. 44, 31–54.

Lam, F.P.A., Maas, L.R.M., Gerkema, T., 2004. Spatial structure of tidal and residual currents as observed over the shelf break in the Bay of Biscay. Deep-Sea Res. 51, 1075–1096.

Large, W.G., McWilliams, J.C., Doney, S.C., 1994. Oceanic vertical mixing: a review and a model with a nonlocal boundary layer parameterization. Rev. Geophys. 32 (4), 363–403.

Mazé, R., 1987. Generation and propagation of non-linear internal waves induced by tide over a continental slope. Cont. Shelf Res. 7, 1079–1104.

Morel, Y., Baraille, R., Pichon, A., 2008. Time splitting and linear stability of the slow part of the barotropic component. Ocean Modell. 23 (3–4), 73–81.

New, A.L., 1988. Internal tidal mixing in the Bay of Biscay. Deep-Sea Res. 35 (5), 691–709.

New, A.L., Pingree, R.D., 1990. Large-amplitude internal soliton packets in the central Bay of Biscay. Deep-Sea Res. 37A (3), 513–524.

New, A.L., Pingree, R.D., 1992. Local generation of internal soliton packets in the central Bay of Biscay. Deep-Sea Res. 39A (9), 1521–1534.

New, A.L., DaSilva, J.C.B., 2002. Remote-sensing evidence for the local generation of internal soliton packets in the central Bay of Biscay. Deep-Sea Res. 49, 915–934.

Pairaud, I.L., Lyard, F., Auclair, F., Letellier, T., Marsaleix, P., 2008. Dynamics of the semi-diurnal and quarter-diurnal internal tides in the Bay of Biscay. Part 1: barotropic tides. Cont. Shelf Res. 28, 1294–1315.

Pichon, A., Mazé, R., 1990. Internal tides over a shelf break: analytical model and observations. J. Phys. Oceanogr. 20, 657–671.

Pichon, A., Correard, S., 2006. Internal tides modeling in the bay of Biscay. Comparisons with observations. Sci. Mar. 70S1, 68–88.

Pingree, R.D., Mardell, G.T., 1985. Solitary internal waves in the Celtic Sea. Prog. Oceanogr. 14, 431–441.

Pingree, R.D., Mardell, G.T., New, A.L., 1986. Propagation of internal tides from the upper slopes of the Bay of Biscay. Nature 321, 154–158.

Pingree, R.D., New, A.L., 1989. Downward propagation of internal tidal energy into the Bay of Biscay. Deep-Sea Res. 36, 735–758.

Pingree, R.D., New, A.L., 1991. Abyssal penetration and bottom reflection of internal tidal energy in the Bay of Biscay. J. Phys. Oceanogr. 21, 28–39.

Pingree, R.D., New, A.L., 1995. Structure, seasonal development and sunglint spatial coherence of the internal tide on the Celtic and Armorican shelves and in the Bay of Biscay. Deep-Sea Res. 42, 245–283.

Renaudie, C., Baraille, R., Morel, Y., Hello, G., Giordani, H., 2009. Adaptation of the vertical resolution in the mixed layer for HYCOM. Ocean Modell. 30 (2–3), 178–189.

Serpette, A., Mazé, R., 1989. Internal tides in the Bay of Biscay: a two-dimensional model. Cont. Shelf Res. 9, 795–821.

Sherwin, T.J., Vlasenko, V.I., Stashchuk, N., Jeans, D.R.G., Jones, B., 2002. Along-slope generation as an explanation for unusually large internal tides. Deep Sea Res. Part I 49, 1787–1799.

Thorpe, S.A., 1998. Nonlinear reflection of internal waves at a density discontinuity at the base of the mixed layer. J. Phys. Oceanogr. 28, 1853–1860.

Xing, J., Davies, A.M., 1996. Processes influencing the internal tide, its higher harmonics, and tidally induced mixing on the Malin-Hebrides shelf. Prog. Oceanogr. 38, 155–204.

Xing, J., Davies, A.M., 1998. A three dimensional model of internal tides on the Malin-Hebrides shelf and shelf edge. J. Geophys. Res. 103, 27 821–27 847.